Construction and Building Materials 327 (2022) 127036

Contents lists available at ScienceDirect

Construction and Building Materials

journal homepage: www.elsevier.com/locate/conbuildmat

Effectiveness of SHCC strips reinforced with glass fiber textile mesh layers for shear strengthening of RC beams: Experimental and numerical assessments

Ahmed T. Baraghith [a], Walid Mansour [b,*], Reda N. Behiry [a], Sabry Fayed [b]

[a] Structural Engineering Dept., Faculty of Engineering, Tanta University, Tanta, Egypt
[b] Civil Engineering Dept., Faculty of Engineering, Kafrelsheikh University, Kafrelsheikh, Egypt

ARTICLE INFO

Keywords:
Reinforced concrete (RC)
Shear strengthening
Strain-hardening cementitious composites (SHCC)
Glass fiber textile mesh (GFTM)
Beams
Crack width
Finite element analysis

ABSTRACT

In the present study, the potential of the use of strain-hardening cementitious composite strips internally reinforced with glass fiber textile mesh layers (GFTM-SHCC) as a strengthening system for shear-critical reinforced concrete (RC) beams is examined. For this purpose, thirteen simply supported beams incorporating two bare control specimens were tested under a three-point loading scheme. The GFTM-SHCC strips were applied inside 20 mm grooves within the beams' substrate so as to prevent the likelihood of premature debonding failure and to significantly enhance the utilization of the adopted strengthening system. The considered key parameters were the layers' number of the GFTM within the SHCC strip (2, 4, or 6), the spacing between GFTM-SHCC strips (90, 150, or 225 mm), the GFTM-SHCC orientation angle (45°, 60°, or 90°), and the strengthening configurations (side-bonded, U-wrapped, or fully-wrapped). Moreover, the location of the strengthening strips relative to the internal stirrups, if they exist, (aligned or un-aligned), was of interest.

The effectiveness of GFTM-SHCC was evaluated in terms of failure patterns, ultimate shear capacity, and the gain in ductility. Experimental results revealed the effective implementation of the GFTM-SHCC strengthening strips in improving the ultimate shear capacity and the deformation characteristics of the tested specimens; however, their behavior relied on the test parameters. The shear carrying capacity and the ductility of the strengthened RC beams using GFTM-SHCC strips were in the range of 47–142% and 21–172%, respectively, higher than their counterpart control specimens. Furthermore, among all strengthening configurations, fully-wrapped strengthened RC beams demonstrated the highest gains in shear capacity, while inclined GFTM-SHCC strips with orientation angles of 45° and 60° outperformed vertical strips significantly. An analytical model to predict the ultimate shear capacity of the strengthened RC beams was derived and verified against the experimental results. To further assess the potential of the GFTM-SHCC strips for the shear strengthening of RC beams, a three-dimensional (3D) non-linear finite element model (FEM) was created using ABAQUS software and verified against the experimental records. After affirmation of the satisfactory predictive performance of the numerical model, a parametric study was performed to compare the shear responses of RC beams strengthened with intermittent GFTM-SHCC strips with continuous ones (strengthened along the whole shear span zone).

1. Introduction

In general, structural elements of reinforced concrete (RC) buildings and bridges, especially beams, are in demand of strengthening and rehabilitation owing to environmental conditions attack, change of the initial use causing increase in the applied loads, or structural upgrading to follow and apply the new requirements of design codes and guidelines [1]. In the last few decades, composite cement-based mortar reinforced with textile fibers has been widely approved as an appropriate technique for shear strengthening of RC structural elements [2]. In the literature, numerous studies have been conducted to describe the behavior of such composite materials depending on the cementitious matrix and fibers utilized, including textile reinforced concrete (TRC) [3–5], textile reinforced mortar (TRM) [6–8], fiber reinforced concrete (FRC) [9–13], mineral-based composites (MBC) [14], and fiber reinforced cementitious matrix (FRCM) [15–17].

* Corresponding author at: Civil Engineering Dept., Faculty of Engineering, Kafrelsheikh University, Kafrelsheikh 33511, Egypt.
E-mail address: waled_mansour@eng.kfs.edu.eg (W. Mansour).

https://doi.org/10.1016/j.conbuildmat.2022.127036
Received 23 November 2021; Received in revised form 6 February 2022; Accepted 1 March 2022
Available online 7 March 2022
0950-0618/© 2022 Elsevier Ltd. All rights reserved.

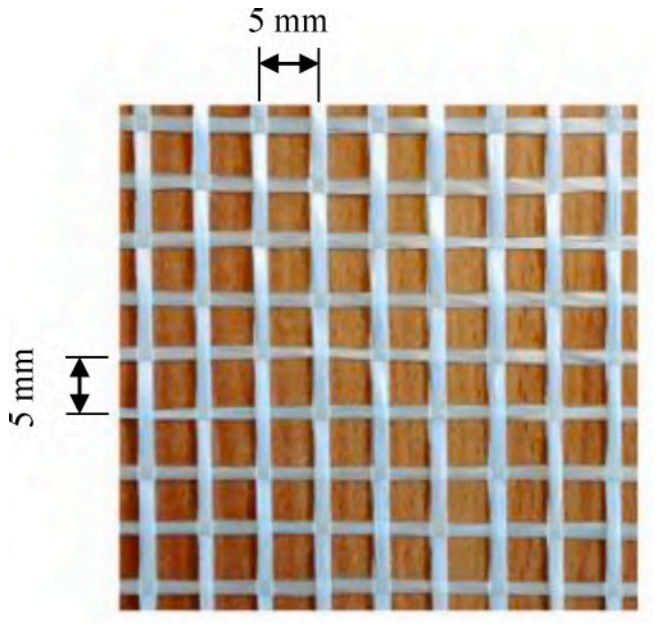


Fig. 1. The used glass fiber textile mesh (GFTM).

Table 1
Geometric and mechanical properties of the used GFTM.

One layer nominal thickness (mm)	E_f (GPa)	f_f (MPa)	ε_{uf} (%)
0.12	70	900	1.20

In the unidirectional case, the properties given are in the principal direction of the reinforcement, modulus of elasticity (E_f), ultimate tensile strength (f_f), ultimate strain (ε_{uf}).

Several variables were previously examined when experimentally investigating the shear strengthening of RC beams using TRM composites. The number of the strengthening layers significantly affected the shear capacity and the failure mode of the tested RC beams [18]. Tetta et al. [19] compared the shear responses of RC beams either strengthened with one or two TRM layers. Doubling the number of layers (two layers) increased the shear capacity by 2.6 times with respect to one TRM layer and changed the failure pattern to debonding of the TRM layers in which a thin layer of concrete was attached instead of fibers rupture in the case of one TRM layer being applied. In order to prevent the debonding of the strengthening TRM layers so as to achieve a significant enhancement in the shear performance of the tested RC beams, TRM end strips anchorage systems were suggested by Raoof et al. [20]. Contrary to expectations, the results were disappointing, as the strengthening efficiency was only enhanced by 9% compared to the non-anchored specimen, because even if the TRM debonding was delayed, a full composite interaction did not occur due to slippage of the textile fibers at the joint where the TRM layers meet the anchorage strips.

To the authors' best knowledge, few available previous studies experimentally investigated the effects of strengthening configurations (side-boned, U-wrapped, and fully-wrapped TRM jackets) on the crack's propagation and ductility of shear-strengthened RC beams [7,17,21–23]. Further experimental and numerical investigations are necessarily required to accurately analyze the shear responses of RC beams strengthened with different configurations, especially if the concluded results contradict each other. Specifically, Azam and Soudki [24] showed that both side-bonded and U-wrapped TRM jackets exhibited identical shear capacities, while the results of Tetta et al. [19] displayed that RC specimens strengthened with U-wrapped jackets had a remarkable increase in the total load-carrying capacity with respect to their counterparts strengthened with only side-bonded jackets.

It is noticed that the majority of the previous studies concerned with strengthening RC beams using vertical TRM jackets. Regarding the strengthening orientation, few experimental investigations have explored the inclination of the TRM layers [21,25], despite the results indicated that the gain in ultimate load was higher for inclined TRM strips at 45° than that strengthened with vertical strips [25]. Additional experimental studies have become mandatory to show the extent to which the inclination angle of the TRM strips affect the shear performance of strengthened RC beams. Another parameter examined in previous studies was the amount of internal stirrups as shear reinforcements [26–27] while impacts of spacing between the TRM strengthening layers were rarely considered.

For the purpose of handling the above-mentioned limitations and for discovering the most optimal strengthening techniques, numerical attempts are urgently required to develop new strengthening systems. Numerical studies found in previous research studies, though rare, have merely predicted the shear capacity of the tested specimens using ABAQUS/Standard [28] or only focused on strengthening specimens with more numbers of TRM layers using LS-DYNA [29].

Currently, a great attention is paid on new category of fiber reinforced cementitious composites called strain-hardening cementitious composites (SHCC) owing to their higher damage tolerance capacity, ductility, and durability. In regard, this explains the ongoing rapid spread of SHCC in the structural applications as a strengthening material [30–37]. Based on the above background survey, it can be found that most of the earlier studies used a normal strength mortar as cementitious matrix for the TRM composites. Consequently, this paper goes several steps beyond the current state of the art by reinforcing SHCC with glass fiber textile mesh (GFTM) in order to exploit the advantages of ductile and strain-hardening response of SHCC under tensile loading conditions instead of the tension-softening criteria governed the behavior of ordinary fiber-reinforced composites.

The main objective of the current experimental program is to show the effects of: (1) the number of GFTM layers within the SHCC strip; (2) spacing between GFTM-SHCC strips, where the total tensile force of all strengthening strips in the tested shear span was kept constant; (3) the orientation angle of the strengthening system; (4) GFTM-SHCC configuration; and (5) the location of the strengthening strips relative to the internal stirrups, either positioned at the same location as the stirrup legs (aligned) or between them (un-aligned). It is worth mentioning that the GFTM-SHCC strengthening strips were cast inside 20 mm grooves within the web of the RC beams in order to prevent the debonding of the strengthening strips and to considerably improve the utilization of the strengthening process. The experimental variables are carefully considered to cover the limitations found in the literature and to add knowledge as well as better understanding to the field of shear strengthening using GFTM-SHCC strips. An analytical model was developed and validated against the experimental results of the strengthened RC beams. Moreover, a numerical analysis was performed using ABAQUS software to study the shear performance of RC beams strengthened using continuous GFTM-SHCC strips along the whole shear span and make a useful comparison with specimens strengthened using intermittent GFTM-SHCC strips.

2. Test program

2.1. Material properties

The main target of the current study is to investigate the cracking load, shear capacity, stiffness, ductility, crack width, and failure patterns of RC beams strengthened in shear using GFTM-SHCC strips. Glass fiber textile mesh (GFTM) locally produced by Sika Company (Sika fiber mesh 1000) was used as the non-metallic fabric reinforcement for the SHCC strips. The Sika fiber mesh 1000 consists of two-dimensional glass fiber ropes with a rectangular cross section of 0.85 mm in width and 0.12 mm in thickness. As shown in Fig. 1, the mesh spacing between the glass fiber

Table 2
Mix proportions of RC and SHCC materials (kg/m^3).

Mix	W/B*	Cement	Sand	Crushed limestone	Water	Silica fume	Super-plasticizer	PP Fiber (12 mm)
RC	0.50	350	637	1295	175	—	—	—
SHCC	0.27	1090	654	—	327	109	24	12

* W/B is the water/ binder ratio, B = cement + silica fume.

Table 3
Mechanical properties of both RC and SHCC materials.

Mechanical properties	NSC(1)					SHCC				
	Sample (1)	Sample (2)	Sample (3)	Average	STDV	Sample (1)	Sample (2)	Sample (3)	Average	STDV
Compressive strength, MPa [38]	24.8	25.2	25.1	25.0	0.21	80.3	79.8	80.0	80.0	0.25
Splitting tensile strength, MPa [39]	3.42	3.58	3.15	3.38	0.22	6.95	6.60	6.91	6.82	0.19
Flexural strength, MPa [40] and [41]	4.05	4.32	4.25	4.21	0.14	8.19	8.05	7.95	8.06	0.12
Bonding strength between RC and SHCC, MPa [42]	—	—	—	—	—	2.25	2.19	2.05	2.16	0.10

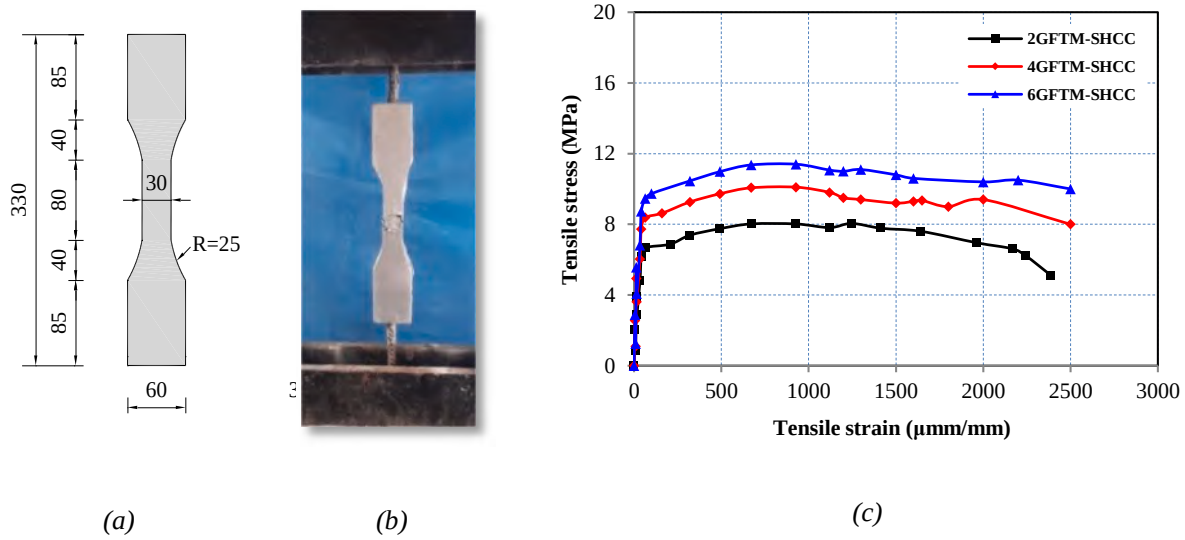


Fig. 2. Uniaxial tensile testing of the dog-bone shaped GFTM-SHCC specimens: (a) dimensions of specimens in mm, (b) test setup, (c) obtained stress–-strain diagrams.

ropes was 5 mm in both directions. According to the manufacturer's data sheet, the weight and the elastic modulus of the glass fiber textile mesh were 74 g/m^2 and 70 GPa, respectively. Moreover, the ultimate tensile strength and the corresponding elongation of the GFTM were 900 MPa and 1.2%, respectively. The mechanical properties of the GFTM as per recommendations of the manufacturer were listed in Table 1.

The strain-hardening cementitious composites (SHCC) strengthening strips were constructed through well mixing of ordinary Portland cement (type I 52.5R), fine aggregates (sand) with maximum aggregate size of 0.5 mm and fine silica fume with average diameter of 0.2 μm. A low water/binder (W/B) ratio of 0.27 was used together with Sika viscocrete superplasticizer (SP) to ensure good workability of the SHCC mixture. The 12 mm length and 0.012 mm in diameter polypropylene (PP) discrete fiber commercially produced by Sika Company was used as internal reinforcement. The used PP fiber had a tensile strength of 400 MPa and an elongation of 80% to match the provisions of strain-hardening response. On the other hand, all RC beams were cast using ready-mixed concrete. The designed strength of concrete was 25 MPa (grade C25). To prepare the concrete mixture, ordinary Portland cement (type I, 42.5R), fine aggregates (sand), coarse aggregates (crushed limestone) with a maximum aggregate size in the range of 10–20 mm and a water/cement ratio of 0.5 without additional additives were used. Design proportions of both RC and SHCC materials were given in Table 2.

During the manufacturing process of RC and SHCC, three cube specimens of 150x150x150 mm for each material were cast from the same patches to record their compressive strengths according to the ECP 203–2018 [38]. Also, three cylinders of 150 mm in diameter and 300 mm in height were prepared to determine the splitting tensile strength of RC and SHCC as per the recommendations of ISRM [39]. Moreover, the flexural strength of the two materials was calculated using three prisms of 40x40x160 mm for each material, based on the recommendations of ASTM-C1609 [40] and Sakr et al. [41]. In order to classify the bond strength between RC and SHCC, a split cylinder test was performed on three composite SHCC-normal concrete cylinders in compliance with ASTM-C496 [42]. After curing at room temperature of 22 ± 2°C for 28 days, all cubes, cylinders, prisms, and composite cylinders were tested to determine the mechanical properties of the RC and SHCC materials. Results showed that the average values of the compressive strength, the flexural strength, and the splitting tensile strength of RC were 25, 4.21, and 3.38 MPa, respectively, whereas these values were 80, 8.06, and 6.82 MPa, respectively, for SHCC materials, as listed in Table 3. Additionally, it was observed that the bonding strength between RC and SHCC was $2.16MPa > 2.1MPa$ which could be classified as excellent bonding according to Sprinkel and Ozyildirim [43] as well as Mansour and Fayed [44].

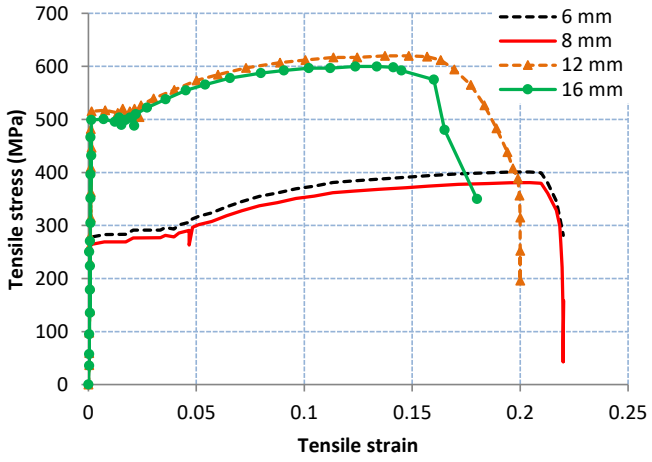


Fig. 3. Tensile stress–strain behaviors for the steel rebars.

Table 4
Properties of the steel reinforcement using uniaxial tensile test.

Diameter Φ (mm)	Yielding strength f_y (MPa)	Ultimate strength f_u (MPa)	Yielding strain ε_y (‰)	Ultimate strain ε_u (‰)
6	280	400	1.40	22.0
8	240	380	1.20	22.0
12	520	620	2.25	20.0
16	490	600	2.10	18.0

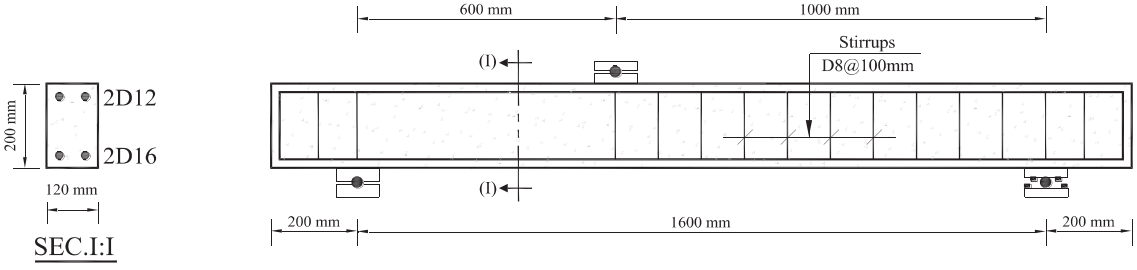
Uniaxial tensile tests were carried out on nine dog-bone shaped specimens in order to record the stress–strain responses of the SHCC strips internally reinforced with 2, 4, and 6 layers of GFTM sheets, as shown in Fig. 2(a) and Fig. 2(b). Three specimens were tested for each number of layers, and the obtained average stress strain curve is plotted in Fig. 2(c). All the tested GFTM-SHCC strips approximately failed at the same strain of 2500 μmm/mm. Moreover, results showed that as the number of GFTM layers increased, the tensile stress of the GFTM-SHCC strips remarkably increased. The ultimate tensile strength of the SHCC strips reinforced with 2, 4, and 6 layers of GFTM was 8.05, 10.1, and 11.4 MPa, respectively. On the contrary, the number of the GFTM layers did not significantly change the elastic modulus of the tested strips.

Four different diameters of steel reinforcement bars were used in the experimental program; 6, 8, 12, and 16 mm. Uniaxial tensile tests were performed on both plain bars with diameters of 6 and 8 mm and ribbed bars with diameters of 12 and 16 mm to obtain the stress–strain responses of the used reinforcements, which are plotted in Fig. 3. For the 6, 8, 12, and 16 mm diameter bars, the yield strength values were 280, 240, 520, and 490 MPa, respectively, while their ultimate strength values were 400, 380, 620, and 600 MPa, respectively. Table 4 shows that the yielding strain of the tested steel rebars ranged from 1.20% to 2.25%, while their ultimate strain was in the range of 18–22%.

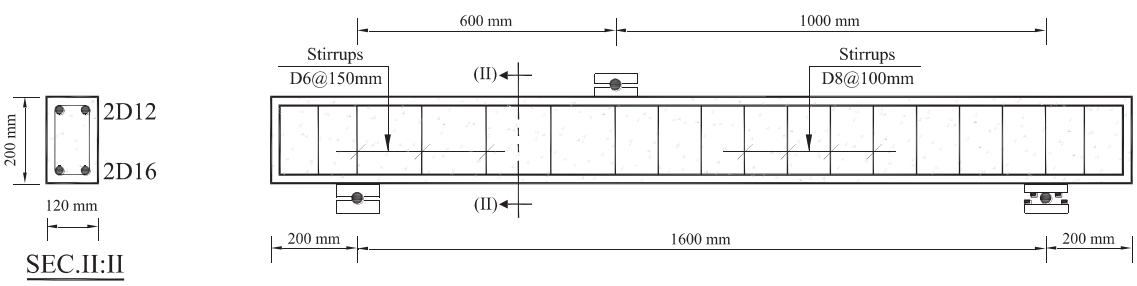
2.2. Design of beams

The experimental test matrix was designed to investigate the shear behavior of RC beams strengthened using GFTM-SHCC strips with different configurations and orientations compared to the un-strengthened specimens. In the current experimental program, a total of thirteen half-scale simply supported RC beams with rectangular cross sections were tested. The concrete cross-sectional area was 120 mm in width × 200 mm in depth. In addition, the tensile and compressive longitudinal reinforcement ratios were identical for all specimens. To ensure shear failure prior to flexural one, 2D16 mm and 2D12 mm high tensile ribbed steel bars were utilized as the tensile and compressive reinforcements, respectively, as per recommendations of the ECP 203–2018 [38].

The total and effective lengths of the tested beams were 2000 and 1600 mm, respectively. The effective length of the tested beams was divided into two parts; the length of the first part was 1000 mm measured from the right support and was internally reinforced with stirrups of 8 mm diameter normal mild steel spaced every 100 mm as



(a) All specimens except BC2, $BT_{4\text{-}150\text{-}UW\text{-}90\text{-}H1}$ and $BT_{4\text{-}150\text{-}UW\text{-}90\text{-}H2}$



(b) Specimens BC2, $BT_{4\text{-}150\text{-}UW\text{-}90\text{-}H1}$ and $BT_{4\text{-}150\text{-}UW\text{-}90\text{-}H2}$

Fig. 4. Geometry and internal steel reinforcements of the tested specimens.

Table 5
Details of test matrix.

Specimen	Characteristics	N	S_m (mm)	θ(degree)	Jacket configuration	Stirrups at the strengthened shear span
BC1	Control specimen without web reinforcement in the strengthened shear span	–	–	–	–	–
BC2	Control specimen with web reinforcement in the strengthened shear span	–	–	–	–	D6@150 mm
$BT_{2\text{-}150\text{-}UW\text{-}90}$	Strengthened specimen using 2 layers of GFTM within U-wrapped vertical SHCC strips.	2	150	90	U-wrapped	–
$BT_{4\text{-}150\text{-}UW\text{-}90}$	Strengthened specimen using 4 layers of GFTM within U-wrapped vertical -SHCC strips.	4	150	90	U-wrapped	–
$BT_{6\text{-}150\text{-}UW\text{-}90}$	Strengthened specimen using 6 layers of GFTM within U-wrapped vertical -SHCC strips.	6	150	90	U-wrapped	–
$BT_{4\text{-}225\text{-}UW\text{-}90}$	Strengthened specimen using U - wrapped vertical GFTM-SHCC strips at spacing 225 mm.	4	225	90	U-wrapped	–
$BT_{4\text{-}90\text{-}UW\text{-}90}$	Strengthened specimen using U - wrapped vertical GFTM-SHCC strips at spacing 90 mm.	4	90	90	U-wrapped	–
$BT_{4\text{-}150\text{-}UW\text{-}60}$	Strengthened specimen using U - wrapped inclined GFTM-SHCC strips at angle 60°.	4	150	60	U-wrapped	–
$BT_{4\text{-}150\text{-}UW\text{-}45}$	Strengthened specimen using U - wrapped inclined GFTM-SHCC strips at angle 45°.	4	150	45	U-wrapped	–
$BT_{4\text{-}150\text{-}SB\text{-}90}$	Strengthened specimen using side-bonded vertical GFTM-SHCC strips.	4	150	90	Side-Bonded	–
$BT_{4\text{-}150\text{-}FW\text{-}90}$	Strengthened specimen with fully-wrapped vertical GFTM-SHCC strips.	4	150	90	Fully-Wrapped	–
$BT_{4\text{-}150\text{-}UW\text{-}90\text{-}H1}$	Strengthened specimen using U - wrapped GFTM-SHCC strips aligned with web reinforcement in the strengthened shear span.	4	150	90	U-wrapped	D6@150 mm (aligned)
$BT_{4\text{-}150\text{-}UW\text{-}90\text{-}H2}$	Strengthened specimen using U - wrapped GFTM-SHCC strips un-aligned with web reinforcement in the strengthened shear span.	4	150	90	U-wrapped	D6@150 mm (un-aligned)

N = Layers' number of the GFTM within the SHCC strip; S_m = spacing between GFTM-SHCC strips; θ = GFTM-SHCC orientation angle.

shear reinforcements to prevent the occurrence of shear failure on the right side of the tested beams even after the left side was strengthened. On the other hand, the second part (600 mm from the left support) had two conditions either kept bare or internally reinforced with stirrups of 6 mm diameter spaced every 150 mm. The tested beams were designed to be ordinary shallow beams according to ASCE-ACI Committee 445 [45] where the shear span to effective depth ratio (a/d) was kept constant at 3.3. A clear 20 mm cover was provided at the bottom and sides of the RC beams. Geometry, dimensions, and layout of the internal steel rebars of the tested RC beams were depicted in Fig. 4.

The subscript ID consisted of four syllables; the first one represented the number of glass fibers textile mesh (GFTM) layers while the second syllable described the spacing between GFTM-SHCC strips. On the other hand, strengthening configurations and orientations were obviously stated by the third and the fourth syllables, respectively. To compose the test program of all strengthened specimens, three different numbers of GFTM layers within the SHCC strips were suggested i.e., 2, 4, and 6 layers with different GFTM-SHCC strips spacing; 90, 150, and 225 mm. Moreover, three configurations were proposed; side-bonded (SB), U-wrapped (UW), and fully-wrapped (FW) in addition to three orientation angles; 45°, 60°, and 90° to the axis of the beam.

Two RC beams were considered as control specimens (without GFTM-SHCC strips); BC1 without internal shear reinforcement at left side (strengthening zone) in adjunct to BC2 with internal stirrups of diameter 6 mm spaced every 150 mm at the strengthened shear span. Nine RC beams ($BT_{2\text{-}150\text{-}UW\text{-}90}$, $BT_{4\text{-}150\text{-}UW\text{-}90}$, $BT_{6\text{-}150\text{-}UW\text{-}90}$, $BT_{4\text{-}225\text{-}UW\text{-}90}$, $BT_{4\text{-}90\text{-}UW\text{-}90}$, $BT_{4\text{-}150\text{-}UW\text{-}60}$, $BT_{4\text{-}150\text{-}UW\text{-}45}$, $BT_{4\text{-}150\text{-}SB\text{-}90}$, and $BT_{4\text{-}150\text{-}FW\text{-}90}$) were strengthened in the tested shear span using GFTM-SHCC strips. It worth mentioning that, no web reinforcements were placed into the strengthened shear zone of these specimens to get an accurate and explicit examination of the studied variables. Additionally, two specimens with web reinforcement (D6@150 mm) in the strengthened shear span were added to the specimen matrix to study the effect of the location of the strengthening strips relative to the internal stirrups. The first one ($BT_{4\text{-}150\text{-}UW\text{-}90\text{-}H1}$) was strengthened using U-wrapped GFTM-SHCC strips positioned at the same location of the stirrup legs (aligned) while in the second specimen ($BT_{4\text{-}150\text{-}UW\text{-}90\text{-}H2}$), the GFTM-SHCC strips were positioned between the stirrups (un-aligned). Table 5 and Fig. 5 show the test matrix as well as the scheme of all strengthened specimens.

2.3. Strengthening procedure

The interface surface preparation between the RC beam substrates and the GFTM-SHCC strengthening strips is considered one of the most important factors affecting the efficiency of the strengthening technique. At application of loads, the separation/debonding of the strengthening layers/strips from the RC beam substrates is one of the best-known failure patterns obtained due to the poor interaction between the two surfaces as well as lower contact areas. Debonding negatively affects the load carrying capacity of the strengthened RC beams. In order to prevent debonding of the GFTM-SHCC strips from the RC beam substrates, roughened grooves of 20 mm depth were manually cut according to the desired strengthening configurations and orientations before casting the GFTM-SHCC strengthening strips as depicted in Fig. 6(a) and 6(b). After making the grooves, the RC beam surface was then grinded and cleaned using air blower as shown in Fig. 6(c). Prior casting the SHCC inside the grooves, the epoxy resin was firstly prepared and applied (Fig. 6(d)). In the current study, MasterBrace 1414 epoxy resin locally produced by BASF Company with the mechanical properties shown in Table 6 was used to connect the strengthening strips and the RC beam surfaces. The MasterBrace 1414 epoxy composed of two components A and B mixed thoroughly using a slow speed mixer fitted with a suitable paddle according to the manufacturer's data sheet to obtain a homogeneous mixture.

In the next step, the GFTM-SHCC strips were installed on the specified sides of the RC beams with the required configurations and orientations by applying the first layer of SHCC mortar using a steel trowel followed by gradually embedding the first layer of GFTM inside the mortar. Subsequently, the second layer of SHCC mortar, the second layer of GFTM, and a finishing SHCC mortar layer were applied as shown in Fig. 6(e) through 6(h). The same procedures were repeated in case of more than two GFTM layers were required. The strengthening process began seven days after the beams were cast. The main targets of the use of epoxy along with SHCC material are (1) to compensate for any loss that may occur in the shear resistance of the concrete section as a result of removing 20 mm of it, (2) to prevent debonding of the strengthening strips as much as possible, and (3) to preserve the original dimensions of

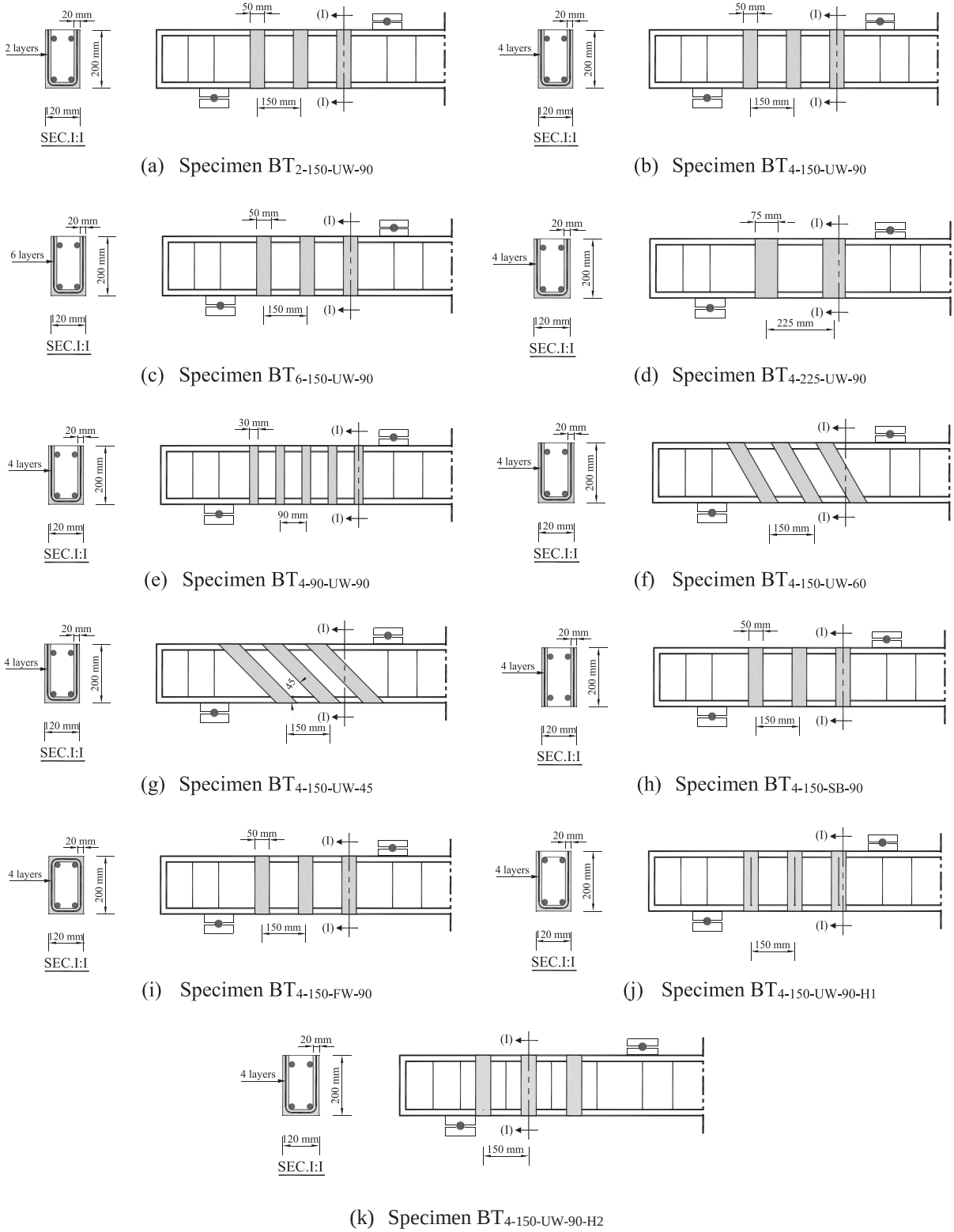


Fig. 5. Scheme of strengthened specimens.

the RC beams. The strengthened RC beams were cured for 28-days prior to testing using a moistened cloth at room temperature.

2.4. Setup

All tested beams either strengthened or kept bare were subjected to monotonic loading under a three-point loading test setup as sketched in Fig. 7. The monotonic load was gradually applied in a force controlled-manner with loading rate of 1.0 kN/min and recorded using a load cell of 500 kN capacity. The vertical deflections at different loading stages were traced using four linear variable differential transformers (LVDTs) positioned at different locations of the tested specimens. Two of them were under the mid-span section and the loading point; whereas, the rest were situated above of the supporting points. The purpose of fixing a



Fig. 6. Strengthening application process.

Table 6
Properties of the used mixed resin.

Compressive strength (MPa)	Tensile strength (MPa)	Slant shear bond (MPa)	Bond strength (MPa)
65.0	25.0	> 11.0	> 2.50

LVDT in the bending zone was not only to record the net-deflection of the tested beams but also to compare the ductility of the tested specimens. Additionally, in order to record both the major shear crack width and the developed shear strains, two 45-degree LVDTs (Rosette) were attached on the RC beam surface at the center of the shear span. Moreover, an electrical steel strain gauge (S1) with 6.0 mm length was installed on the tensile reinforcement at mid-span zone in order to determine the axial strain developed in the longitudinal reinforcement bars. Part of the ripped tensile steel bar was smoothed before installing of the strain gauge to ensure well bonding between the electrical strain gauge and the steel bar. Finally, the compressive strain at mid-span section of the tested specimens was estimated using electrical pi-gauge (PI). Results of Pi-gauge, strain gauge, LVDTs and load cell were collected and stored during testing by using a data acquisition unit, KYOWA model PCD-300A with sampling rate of 5 kHz. The tested beam was rested on two supports; one of them was roller while the other was hinged.

3. Test results

3.1. Failure patterns

Fig. 8 shows the failure patterns for all tested RC beams at ultimate load. Generally, control specimens (un-strengthened beams) as well as GFTM-SHCC strengthened beams exhibited shear failure patterns due to the propagation of major shear crack with or without secondary shear cracks within the shear span region. For all tested RC beams, the flexural cracks first appeared almost under the loading point. Except for the $BT_{4\text{-}90\text{-}UW\text{-}90}$ specimen, all control and strengthened beams failed due to the formation of a major critical shear crack along the diagonal direction connecting the support and loading point. As the applied load increased, the width of the major shear crack was gradually increased in conjunction with the emergence of secondary shear cracks at the critical shear span zone. Due to the minimization of spacing between GFTM-SHCC strengthening strips for specimen $BT_{4\text{-}90\text{-}UW\text{-}90}$, which had the lowest spacing between strengthening strips of 90 mm, the shear strength of the considered beam was significantly improved compared to other specimens. Thus, its failure was governed by the development of two parallel major shear cracks; the first crack started from the support

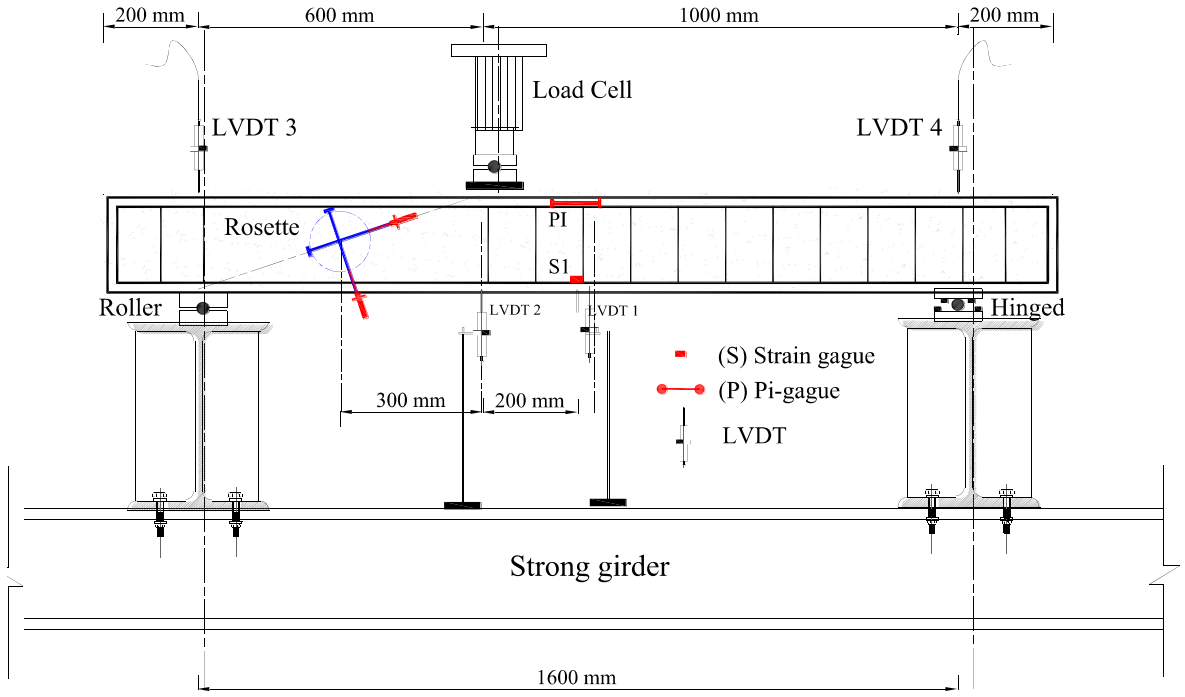


Fig. 7. Test setup and instrumentation.

to the higher mid-point of the critical shear span, while the second one extended from the lower mid-point of the critical shear span to the loading point.

Using a higher number of GFTM layers within the strengthening SHCC strips resulted in a decrease in the obtained major shear crack width at failure compared to a specimen with a lower number of GFTM layers. Moreover, strengthening RC beams using inclined GFTM-SHCC strips approximately perpendicular to the developed shear crack resulted in the appearance of secondary shear cracks in addition to the major one and increased the recorded shear capacity compared to using vertical GFTM-SHCC strips. It is worth mentioning that the proposed strengthening technique (grooves inside the RC beam web) achieved the goal for which it was designed: to prevent debonding/separation between the GFTM-SHCC strengthening strips and the RC beam surfaces. In other words, the failure was controlled by the GFTM-SHCC strip rupture.

3.2. Load-deflection behaviors and ductility of tested beams

The load mid-span deflection behaviors of all test beams at different loading stages are shown in Fig. 9. Furthermore, the net mid-span deflections corresponding to the cracking, yield, and maximum loads (Δ_{cr}, Δ_y and Δ_{max}) are listed in Table 7. For the reader's information, both cracking and maximum deflections were experimentally recorded at cracking and ultimate loads, respectively, while the yielding deflection was theoretically calculated based on the general yielding method recommended by Li et al. [46]; see Fig. 10.

In general, all proposed shear strengthening techniques were efficient in improving both the ultimate shear capacity (V_u) and ductility of tested beams in comparison with the control RC beams. The gains in the ultimate shear capacity ranged between 47% and 142%, while the ductility of strengthened beams was about 21–172% higher than the control beams.

As for reference specimens (BC1 and BC2), results showed that the existence of the shear reinforcement at the critical shear span within the control specimen BC2 delayed the cracking load and remarkably enhanced both the yielding and ultimate loads compared to un-reinforced RC beam BC1. It can be seen in Table 7 that the cracking loads of BC1 and BC2 specimens were 14.5 kN and 18.5 kN, respectively. Also, the yielding and ultimate loads of BC2 were 107% and 115% higher than the control RC beam BC1, respectively. On the other hand, Fig. 9(a) shows that deflections of BC1 and BC2 were approximately identical till cracking while the presence of internal stirrups significantly increased the yielding (Δ_y) and maximum (Δ_{max}) deflections. Therefore, ductility index ($\Delta_{max.}/\Delta_y$) of BC2 was 1.60 compared to 1.36 for BC1 with increasing ratio of 18%. Briefly, usage of the internal stirrups as a shear reinforcement had a satisfactory efficient on crack distribution, delaying cracking load, and significantly increasing both the ultimate shear capacity and ductility compared to un-reinforced specimen.

Regarding to layers' number of the GFTM within the strengthening vertical U-wrapped SHCC at spacing of 150 mm, it can be observed that as the number of GFTM layers increased, the shear performance of the tested RC beams considerably enhanced. As a result, the cracking load was delayed when higher numbers of GFTM layers were used. The cracking loads of specimens $BT_{2\text{-}150\text{-}UW\text{-}90}$, $BT_{4\text{-}150\text{-}UW\text{-}90}$, and $BT_{6\text{-}150\text{-}UW\text{-}90}$ were 19.5, 22.0, and 23.5 kN, respectively. Using 6 layers of GFTM within the SHCC strips (Specimen $BT_{6\text{-}150\text{-}UW\text{-}90}$) demonstrated the highest gains in both ultimate shear capacity and ductility index. This is because the fact that as using higher numbers of GFTM layers increased the tensile strength of the strengthening SHCC strips as previously discussed in Fig. 2. The highest gain in the ultimate shear capacity recorded for specimen $BT_{6\text{-}150\text{-}UW\text{-}90}$ which was about 142% corresponding to the highest number of GFTM (6 layers) in comparison with 47% and 90% for $BT_{2\text{-}150\text{-}UW\text{-}90}$ and $BT_{4\text{-}150\text{-}UW\text{-}90}$, respectively. The same response was obtained regarding the gains in ductility. Values of the ductility index of specimens $BT_{2\text{-}150\text{-}UW\text{-}90}$, $BT_{4\text{-}150\text{-}UW\text{-}90}$, and $BT_{6\text{-}150\text{-}UW\text{-}90}$ were 54, 105, and 127%, respectively, compared to BC1.

Pertaining to spacing between GFTM-SHCC strips, comparison between specimens $BT_{4\text{-}225\text{-}UW\text{-}90}$, $BT_{4\text{-}150\text{-}UW\text{-}90}$, and $BT_{4\text{-}90\text{-}UW\text{-}90}$ with GFTM-SHCC strips of spacing 225, 150, and 90 mm, respectively declared that the spacing between the GFTM-SHCC strips did not significantly affect the cracking load of the strengthened RC beams. Specimens $BT_{4\text{-}225\text{-}UW\text{-}90}$, $BT_{4\text{-}150\text{-}UW\text{-}90}$, and $BT_{4\text{-}90\text{-}UW\text{-}90}$ cracked at 20.5, 22.0, and 24.0 kN, respectively. Quite the contrary, the gain in ultimate shear capacity was considerable when a small spacing (90 mm) between the GFTM-SHCC strengthening strips was suggested. The gain

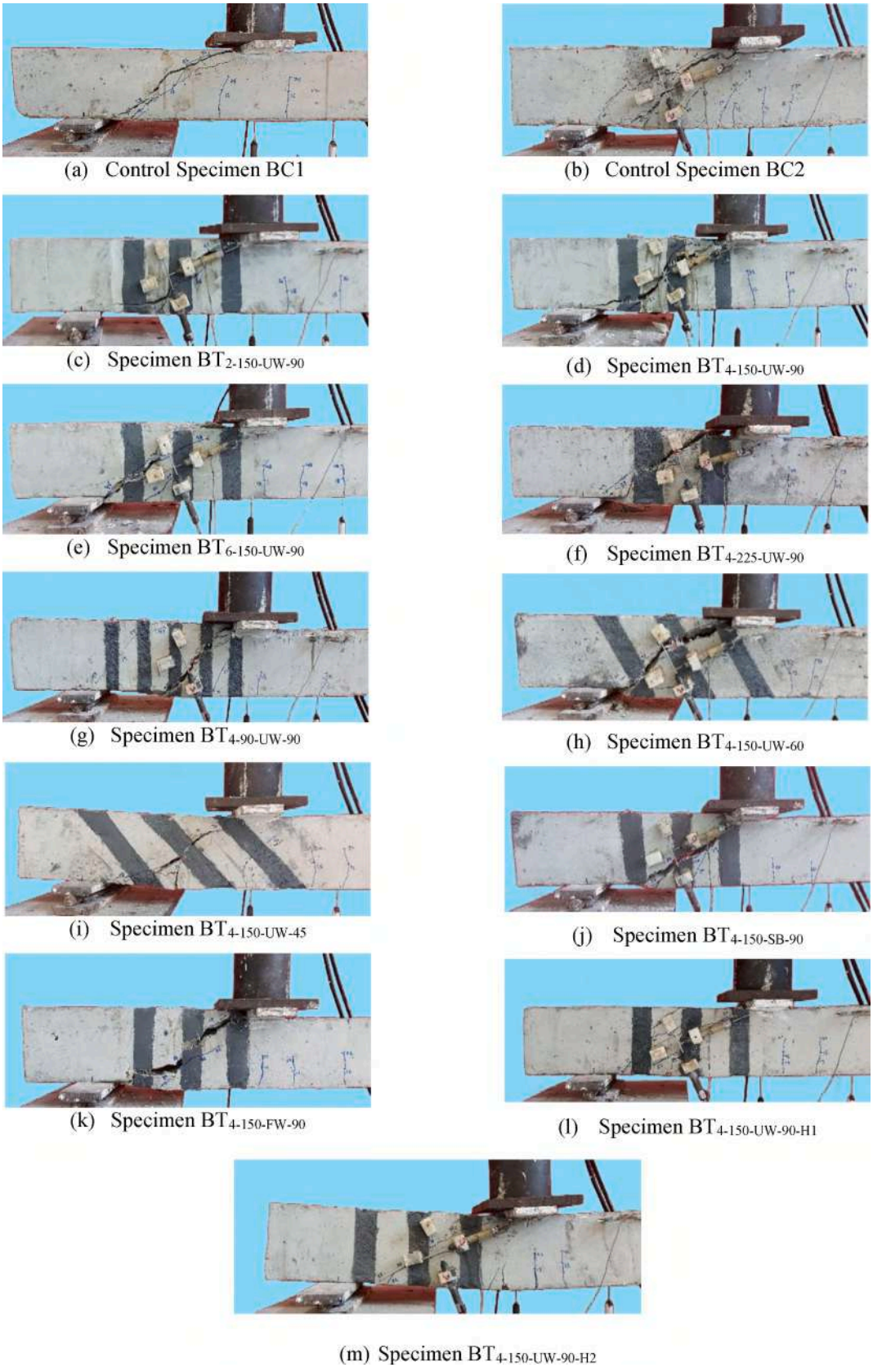
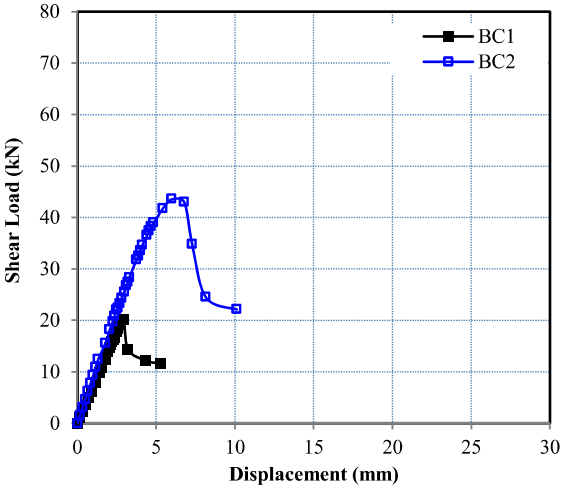
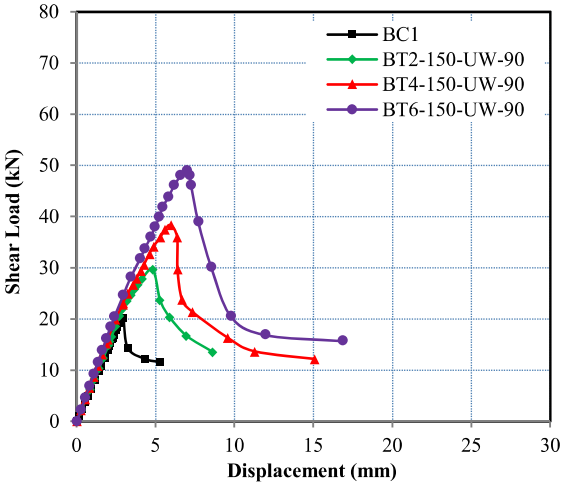


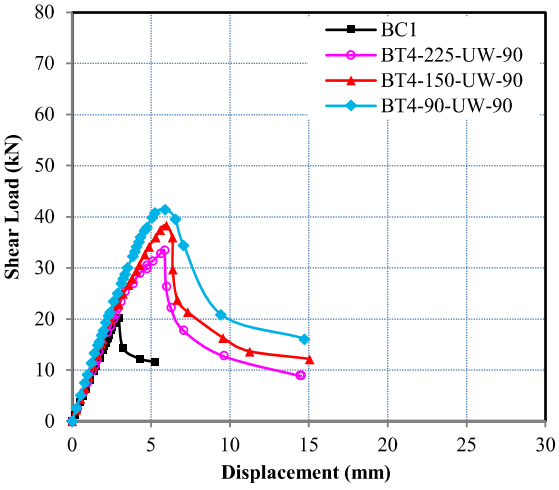
Fig. 8. Failure mode for all tested specimens.



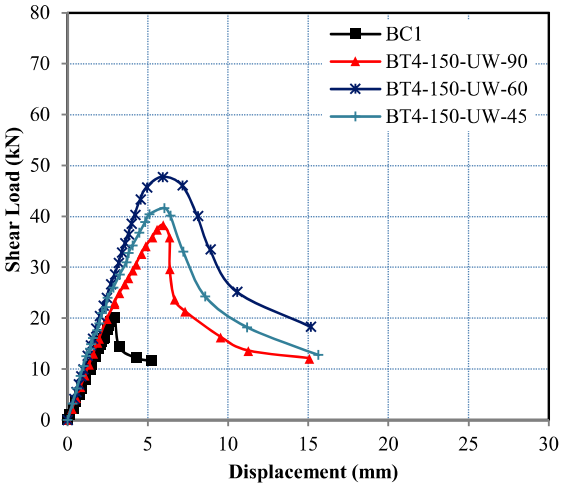
(a) Control specimens



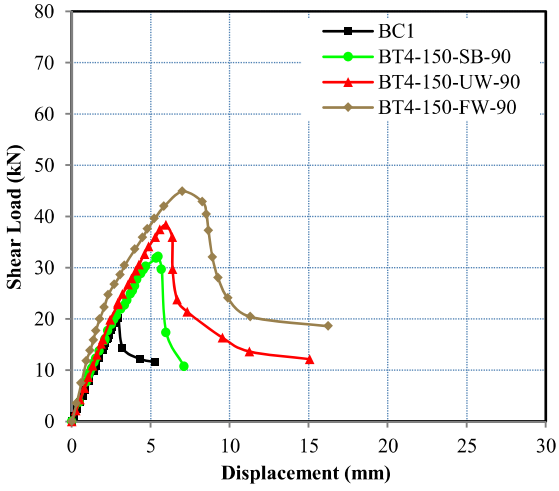
(b) Effect of number of GFTM layers within the SHCC strip



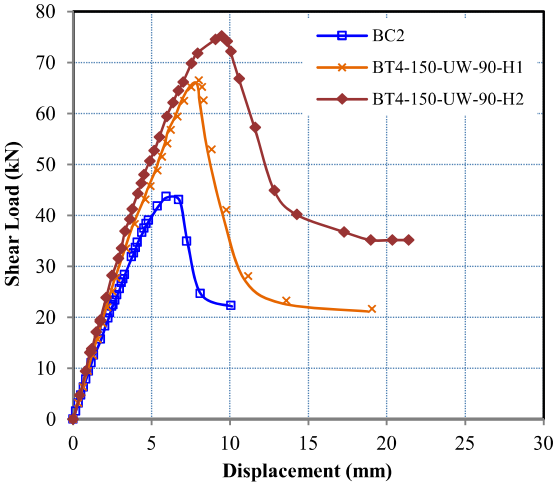
(c) Effect of spacing between GFTM-SHCC strips



(d) Effect of orientation angle of GFTM-SHCC strips



(e) Effect of GFTM-SHCC configuration



(f) Effect of the location of GFTM-SHCC strips relative to the internal stirrups

Fig. 9. Effect of different parameters on load–deflection responses.

Table 7
Experimental results of loads and deflections at different stages.

Specimen	Shear capacities (kN)				Mid-span deflections (mm)			Ductility		Maximum strain (μmm/mm)			
	V_{cr}	V_y	V_u	Gain %	Δ_{cr}	Δ_y	$\Delta_{max.}$	μ_Δ	Gain%	Steel		Concrete	
										ε_s**	Gain%	ε_c ***	Gain %
BC1	14.5	19.9	20.2	NA	2.05	3.87	5.26	1.36	NA	509	NA	−435	NA
BC2	18.5	41.2	43.5	NA	2.07	6.32	10.12	1.60	NA	862	NA	−741	NA
$BT_{2\text{-}150\text{-}UW\text{-}90}$	19.5	28.3	29.7	47	2.70	4.12	8.62	2.10	54	989	94	−588	35
$BT_{4\text{-}150\text{-}UW\text{-}90}$	22.0	36.5	38.3	90	2.92	5.40	15.07	2.79	105	1198	135	−669	54
$BT_{6\text{-}150\text{-}UW\text{-}90}$	23.5	47.4	48.9	142	2.94	5.45	16.85	3.09	127	1228	141	−707	63
$BT_{4\text{-}225\text{-}UW\text{-}90}$	20.5	30.8	33.4	65	2.38	4.87	14.51	2.98	119	1062	109	−652	50
$BT_{4\text{-}90\text{-}UW\text{-}90}$	24.0	40.3	41.5	105	2.89	4.13	14.72	3.56	162	1244	144	−719	65
$BT_{4\text{-}150\text{-}UW\text{-}60}$	26.0	45.9	47.8	136	2.95	4.39	15.12	3.44	153	1296	155	−728	67
$BT_{4\text{-}150\text{-}UW\text{-}45}$	24.5	39.3	41.6	106	2.82	4.91	15.63	3.18	134	1283	152	−715	64
$BT_{4\text{-}150\text{-}SB\text{-}90}$	20.0	30.5	32.2	59	2.36	4.31	7.11	1.65	21	1302	156	−733	69
$BT_{4\text{-}150\text{-}FW\text{-}90}$	26.5	38.6	44.9	122	2.98	4.38	16.22	3.70	172	1322	160	−737	60
$BT_{4\text{-}150\text{-}UW\text{-}90\text{-}H1}$	29.0	64.0	66.1	52*	3.09	6.19	18.78	3.03	89*	1561	81*	−852	15*
$BT_{4\text{-}150\text{-}UW\text{-}90\text{-}H2}$	31.5	71.6	75.2	73*	3.28	5.88	21.37	3.63	127*	1675	94*	−915	24*

V_{cr} is the cracking shear capacity, V_y is the yield shear capacity and calculated based on the general yielding method recommended by Li et al. [46], V_u is the ultimate shear capacity, Δ_{cr} is the deflection corresponding to the cracking load, Δ_y is the deflection corresponding to the yielding load, Δ_{max} is the deflection corresponding to the failure load, μ_Δ is the ductility index and equal to (Δ_{max} / Δ_y), ε_s is the Maximum tensile strain in main reinforcement (μmm/mm), ε_c is the Maximum compression strain in concrete (μmm/mm), and * The values were calculated with respect to the control specimen (BC2).

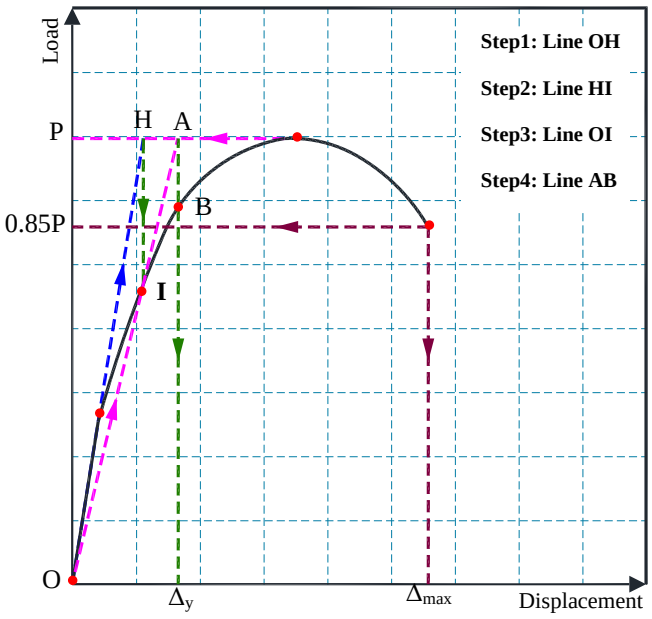


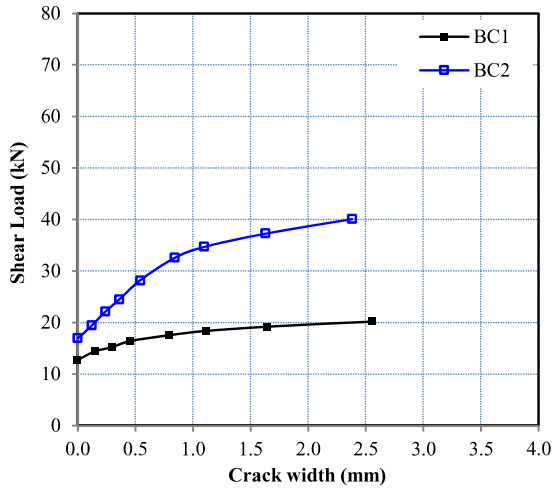
Fig. 10. Definition of yield displacement using general yielding method [46].

in shear capacity of $BT_{4\text{-}225\text{-}UW\text{-}90}$, $BT_{4\text{-}150\text{-}UW\text{-}90}$, and $BT_{4\text{-}90\text{-}UW\text{-}90}$ was 65, 90, and 105%, respectively, with respect to the reference beam BC1. The highest increase in shear capacity was corresponded to the lowest spacing between the GFTM-SHCC strengthening strips. This may be referred to the cracking and failure patterns of the tested RC beam. For specimen $BT_{4\text{-}90\text{-}UW\text{-}90}$, the vertical GFTM-SHCC strengthening strips with 90 mm spacing were able to prevent the continuity of the major shear crack at the critical shear zone. As a result, two thin parallel shear cracks were developed, and the final collapse of the tested specimens was delayed. The importance of using lower strengthening spacing was shown not only in recording a remarkable increase in the ultimate load carrying capacity but also in reducing the mid-span deflections at different stages in terms of cracking, yielding, and ultimate loads. Furthermore, specimen $BT_{4\text{-}90\text{-}UW\text{-}90}$ exhibited the highest gain in ductility among all tested RC beams, 162% higher than the opponent value of the control beam.

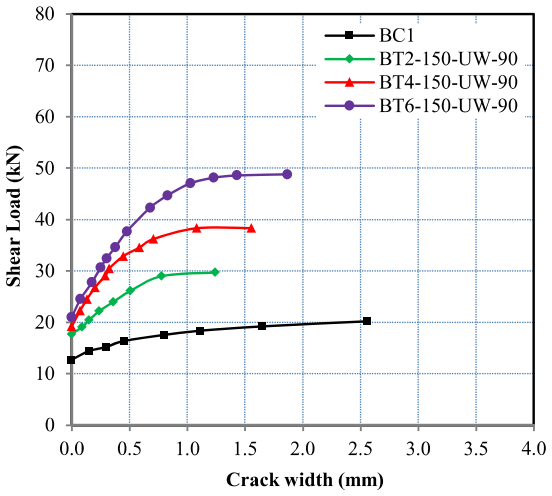
Considering the orientation of the strengthening GFTM-SHCC strips, strengthening RC beams using U-wrapped inclined GFTM-SHCC strips with an orientation angle of 45° and 60° to the axis of the beam has led to a significant improvement in the cracking and ultimate loads compared to 90° (vertical strips). The existence of intermittent inclined strengthening strips approximately perpendicular to the major shear cracks remarkably decreased the yielding mid-span deflection, causing a significant increase in the gain ductility in comparison with vertical strips. Cracking loads of specimens $BT_{4\text{-}150\text{-}UW\text{-}45}$, $BT_{4\text{-}150\text{-}UW\text{-}60}$, and $BT_{4\text{-}150\text{-}UW\text{-}90}$ were 24.5, 26.0, and 22.0 kN, respectively, while their ultimate loads were 41.6, 47.8, and 38.3 kN, respectively. The gain in ductility of $BT_{4\text{-}150\text{-}UW\text{-}45}$, $BT_{4\text{-}150\text{-}UW\text{-}60}$, and $BT_{4\text{-}150\text{-}UW\text{-}90}$ RC beams with respect to the control specimen BC1 was 134, 153, and 105%, respectively. The existence of inclined GFTM-SHCC strengthening strips played an important role in controlling the cracks propagations as well as enhancing the gain in ductility compared to strengthening by using vertical GFTM-SHCC strips.

Regarding the configuration of the strengthening GFTM-SHCC strips, it can be noticed that there was no significant variance in the cracking load of side-bonded and U-wrapped specimens contrary to fully-wrapped RC beams that cracked at higher load. Cracking loads of specimens $BT_{4\text{-}150\text{-}SB\text{-}90}$, $BT_{4\text{-}150\text{-}UW\text{-}90}$, and $BT_{4\text{-}150\text{-}FW\text{-}90}$ were 20.0, 22.0, and 26.5 kN. As expected, the configuration of GFTM-SHCC strengthening strips had incredible impact on the ultimate shear capacity. As the contact area between the strengthening strips and RC beams increased, the gain in ultimate load increased. Specimen $BT_{4\text{-}150\text{-}FW\text{-}90}$ recorded the highest gain in both ultimate load and ductility equal to 122% and 172%, respectively, compared to BC1 due to the full confinement of the RC beam cross-section. Also, U-wrapping strengthening technique (Specimen $BT_{4\text{-}150\text{-}UW\text{-}90}$) achieved significant gain in both ultimate load and ductility. On the other hand, specimen $BT_{4\text{-}150\text{-}SB\text{-}90}$ yielded the lowest gain in ultimate shear capacity and ductility due to the insufficient bond area between the substrate RC beam and the strengthening GFTM-SHCC strips. The gain in ultimate load capacity and ductility was only 59% and 21%, respectively, with respect to the control specimen BC1. Side-bonded strengthening technique failed to remarkably enhance the shear performance of the tested RC beams compared to U-wrapped and full-wrapped strengthening patterns.

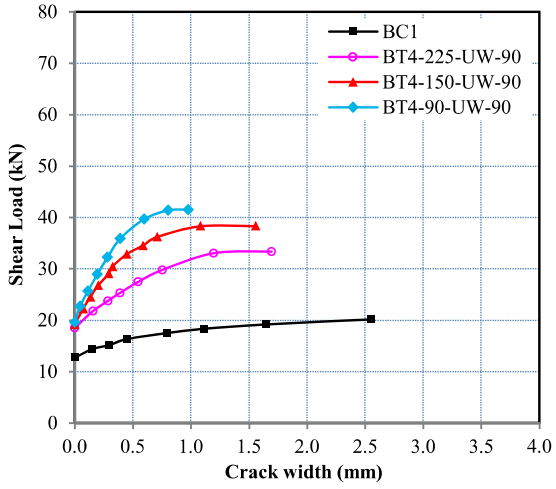
With respect to the location of the strengthening U-wrapped vertical GFTM-SHCC strips relative to the internal stirrups, it can be perceived that the un-alignment of GFTM-SHCC strips with the stirrup legs (specimen $BT_{4\text{-}150\text{-}UW\text{-}90\text{-}H2}$) showed superior increase in the cracking, yielding and ultimate loads compared to specimen $BT_{4\text{-}150\text{-}UW\text{-}90\text{-}H1}$ where the GFTM-SHCC strips were aligned with the stirrups. The gain in ultimate shear capacity of specimens $BT_{4\text{-}150\text{-}UW\text{-}90\text{-}H1}$ and $BT_{4\text{-}150\text{-}UW\text{-}90\text{-}H2}$ was 52% and 73%, respectively, compared to the control specimen



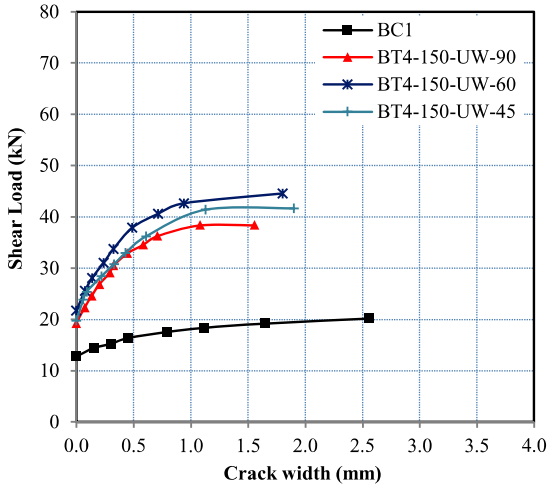
(a) Control specimens



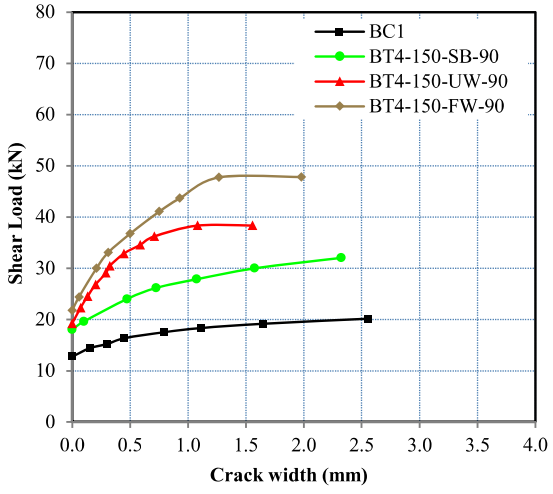
(b) Effect of number of GFTM layers within the SHCC strip



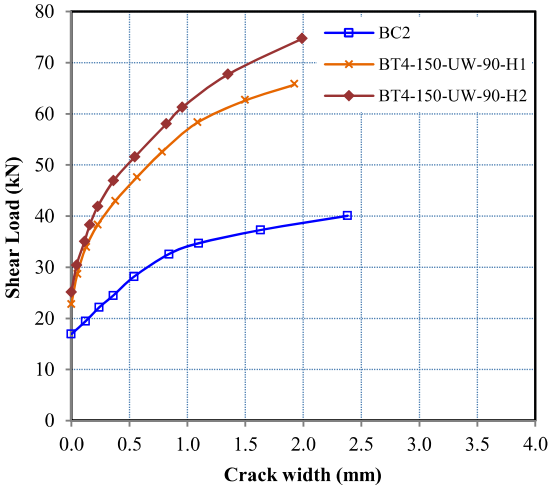
(c) Effect of spacing between GFTM-SHCC strips



(d) Effect of orientation angle of GFTM-SHCC strips

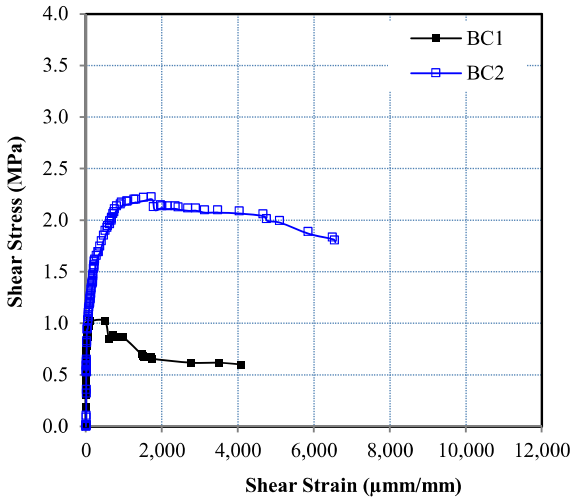


(e) Effect of GFTM-SHCC configuration

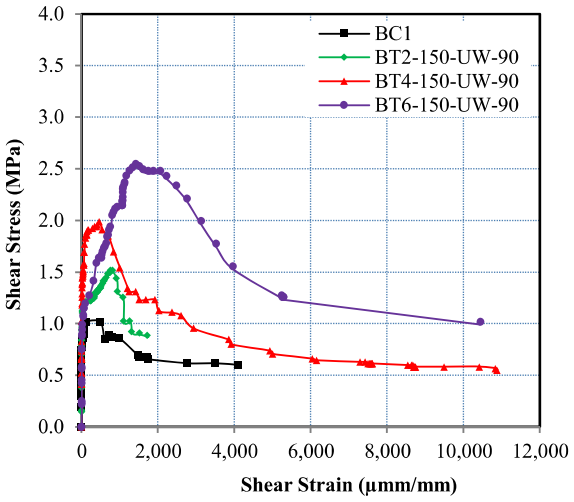


(f) Effect of the location of GFTM-SHCC strips relative to the internal stirrups

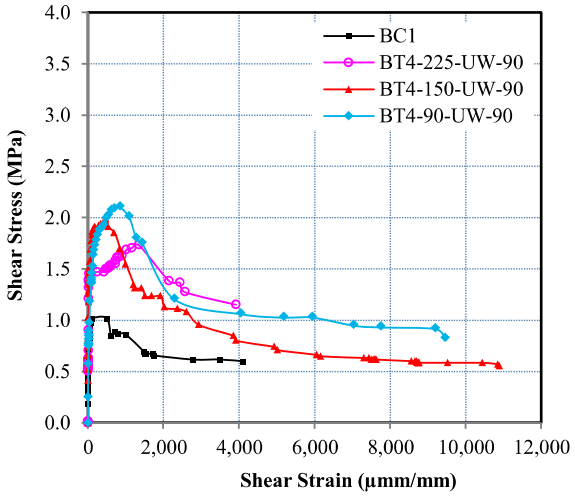
Fig. 11. Effect of different parameters on load-crack width behaviors.



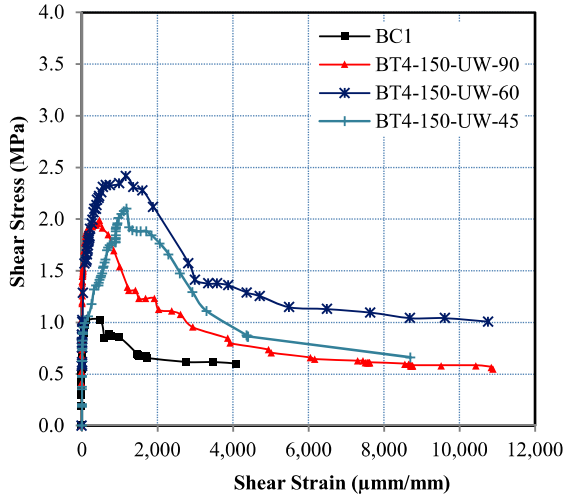
(a) Control specimens



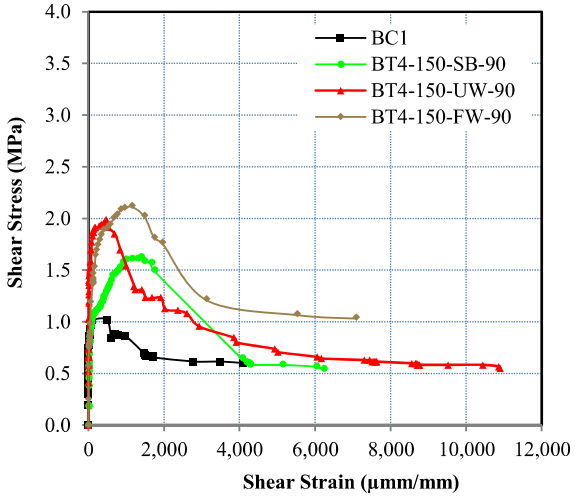
(b) Effect of number of GFTM layers within the SHCC strip



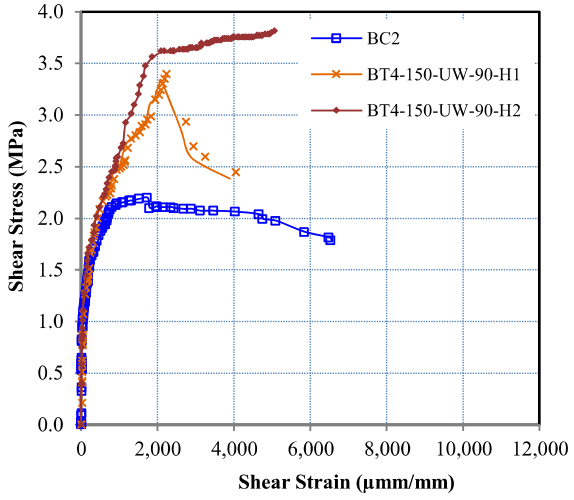
(c) Effect of spacing between GFTM-SHCC strips



(d) Effect of orientation angle of GFTM-SHCC strips



(e) Effect of GFTM-SHCC configuration



(f) Effect of the location of GFTM-SHCC strips relative to the internal stirrups

Fig. 12. Effect of different parameters on shear stress-shear strain relationships.

Table 8
Test results of shear strains at ultimate capacity and failure.

Specimen	Shear strain at V_u (μmm/mm)	Gain %	Shear strain at failure (μmm/mm)	Increase/ decrease %
BC1	113	NA	4903	NA
BC2	1752	NA	6565	NA
$BT_{2\text{-}150\text{-}UW\text{-}90}$	837	641	1752	−64
$BT_{4\text{-}150\text{-}UW\text{-}90}$	485	329	10,897	122
$BT_{6\text{-}150\text{-}UW\text{-}90}$	1422	1159	10,433	112
$BT_{4\text{-}225\text{-}UW\text{-}90}$	1342	1087	3915	−21
$BT_{4\text{-}90\text{-}UW\text{-}90}$	849	651	9462	93
$BT_{4\text{-}150\text{-}UW\text{-}60}$	1193	956	10,783	120
$BT_{4\text{-}150\text{-}UW\text{-}45}$	1186	950	8704	78
$BT_{4\text{-}150\text{-}SB\text{-}90}$	1375	1117	6214	27
$BT_{4\text{-}150\text{-}FW\text{-}90}$	1158	925	7082	44
$BT_{4\text{-}150\text{-}UW\text{-}90\text{-}H1}$	2000	14*	3386	−48*
$BT_{4\text{-}150\text{-}UW\text{-}90\text{-}H2}$	5018	186*	5125	–22*

* The values were calculated with respect to the control specimen (BC2),.

BC2. This was due to the increase in the contact shear area which has been extended to cover most of the critical shear zone area using inner stirrups and GFTM-SHCC strips at different locations rather than confinement of the same points internally by web reinforcements and externally by GFTM-SHCC strips. The gain in ductility of $BT_{4\text{-}150\text{-}UW\text{-}90\text{-}H1}$ and $BT_{4\text{-}150\text{-}UW\text{-}90\text{-}H2}$ was 89% and 127%; respectively, relative to the reference beam BC2. Both specimens succeeded to distribute the shear cracks along the whole critical shear area causing large numbers of thin cracks contrary to other specimens failed due to opening of major shear crack. Generally, strengthening RC beams in shear by vertical GFTM-SHCC strips between the stirrup legs were more efficient than using the strengthening strips at the same location of the stirrup legs.

Specimen $BT_{2\text{-}150\text{-}UW\text{-}90}$ recoded the lowest ultimate shear capacity among all strengthened RC beams due to insufficient numbers of GFTM layers within the strengthening SHCC strips. Although specimen $BT_{4\text{-}150\text{-}SB\text{-}90}$ strengthened with four GFTM layers within the strengthening SHCC strips, the lowest gain in ductility was achieved due to the insufficient anchorage length between the substrate RC beam and the strengthening strips. On the contrary, specimen $BT_{4\text{-}150\text{-}FW\text{-}90}$ exhibited the highest gain in ductility among all strengthened RC beams due to complete bond interaction between the RC beam and the strengthening strips (fully-wrapped strengthening).

3.3. Load-crack width behavior

For all tested specimens, shear load-crack width relationships were plotted in Fig. 11. The results showed that, before the cracking load, both control RC beams (BC1 and BC2) had identical behavior. After reaching the cracking loads, it was obvious that using inner stirrups at the critical shear span (reference specimen BC2) efficiently decreased the crack width of the major shear crack as compared to control specimen BC1. At about 18 kN, the measured shear crack width for specimens BC1and BC2 were 0.797 mm, and 0.098 mm, respectively.

It can be observed that, at all loading levels, GFTM-SHCC strips were efficient to reduce the crack width with respect to the control specimens. Due to the strain-hardening phenomena and the fibers bridging action, the GFTM-SHCC strips prevented the cracks propagations and limited the crack width growth. This observation indicates the effective implementation of the GFTM-SHCC strips in improving the serviceability characteristics of the strengthened specimens. Specifically, strengthening RC beams using a large number of GFTM layers within the SHCC strips exhibited a considerable reduction in the shear crack width as compared to those of the reference specimens owing to the extra-contribution of GFTM. For instance, the shear crack width was higher for specimen $BT_{2\text{-}150\text{-}UW\text{-}90}$ (0.780 mm) than that for specimen $BT_{4\text{-}150\text{-}UW\text{-}90}$ (0.292 mm), which was in turn higher than that for specimen $BT_{6\text{-}150\text{-}UW\text{-}90}$ (0.248 mm) at the same load (29 kN). Moreover, as the strip's spacing was increased, the crack arresting action of the GFTM-SHCC was decreased. Thus, at a load level of about 29 kN, the recorded shear crack widths were wider for specimen $BT_{4\text{-}225\text{-}UW\text{-}90}$ (0.754 mm) than those recorded for specimens $BT_{4\text{-}150\text{-}UW\text{-}90}$ (0.292 mm) and $BT_{4\text{-}90\text{-}UW\text{-}90}$ (0.194 mm).

As for the GFTM-SHCC strip's orientation, the crack widths were reduced when using inclined strips as compared to those when using vertical strips. This may be attributed to the fact that when the GFTM-SHCC strip's inclination angle was near to the direction of principle stresses, their efficiency in restricting the developed cracks improved. For instance, specimen $BT_{4\text{-}150\text{-}UW\text{-}90}$ showed a crack width of 1.080 mm, while specimens $BT_{4\text{-}150\text{-}UW\text{-}45}$ and $BT_{4\text{-}150\text{-}UW\text{-}60}$ displayed a crack width of 0.822 mm and 0.448 mm, respectively, at the same load (38 kN). On the other hand, wider major cracks were developed when only strengthening the RC beam sides (side-bonded) was employed, which may be attributed to the decrease in the anchorage length between the strengthening strips and substrate RC beams. For illustration, at a load of about 29 kN, the crack widths of specimens $BT_{4\text{-}150\text{-}SB\text{-}90}$, $BT_{4\text{-}150\text{-}UW\text{-}90}$, and $BT_{4\text{-}150\text{-}FW\text{-}90}$ were 1.475 mm, 0.324 mm, and 0.210 mm, respectively. Referring to the location of the GFTM-SHCC strips relative to the internal web reinforcement, crack widths of $BT_{4\text{-}150\text{-}UW\text{-}90\text{-}H1}$ (strips aligned with stirrups) and $BT_{4\text{-}150\text{-}UW\text{-}90\text{-}H2}$ (strips un-aligned with stirrups) at a load level of about 38 kN were 0.225 and 0.162 mm, respectively, compared to 1.628 mm for BC2.

3.4. Strains responses

3.4.1. Tensile and compressive strains

The Results of the maximum tensile strain in steel and the maximum compressive strain in concrete for control and strengthened RC beams listed in Table 7 reflect the efficiency of the proposed strengthening techniques. All strengthened RC beams exhibited a higher increase in the axial strain of the longitudinal steel bars than the control specimens; however, the recorded strains (ranging between 989 and 1675 μmm/mm) were much lower than their yielding strain (2100 μmm/mm).

Maximum compressive strain in concrete indicated that the GFTM-SHCC strengthening strips significantly delayed the crack propagation and controlled the width of the major shear crack, which remarkably increased the compressive strain in concrete. RC beams strengthened using GFTM-SHCC strips, without web reinforcement in the shear zone, failed with compressive strain in concrete in the range of 588 to 737 μmm/mm compared to 435 μmm/mm for the control specimens BC1. On the other hand, specimens $BT_{4\text{-}150\text{-}UW\text{-}90\text{-}H1}$ and $BT_{4\text{-}150\text{-}UW\text{-}90\text{-}H2}$ with web reinforcements in the strengthened shear zone achieved the highest compressive strains among all tested specimens. The maximum compressive strains in concrete of BC2, $BT_{4\text{-}150\text{-}UW\text{-}90\text{-}H1}$, and $BT_{4\text{-}150\text{-}UW\text{-}90\text{-}H2}$ were 741, 852, and 915 μmm/mm, respectively.

3.4.1.1. Shear strains. The developed shear strains on the concrete surface of each RC beam were determined using side-bonded LVDTs according to Khalil et al. [47] by means of Eq. (1).

$$\gamma = \frac{\delta_2 - \delta_1}{\sqrt{L_1^2 + L_2^2}} \quad (1)$$

where γ is the developed shear strain; $\delta_2 and \delta_1$ are the LVDT's reading in the direction parallel and perpendicular to the developed major shear crack, respectively, $L_1 and L_2$ are the distances between the fixed points of the LVDTs ($L_1 = L_2 = 120$mm).

Relationships between the shear stress and the calculated shear

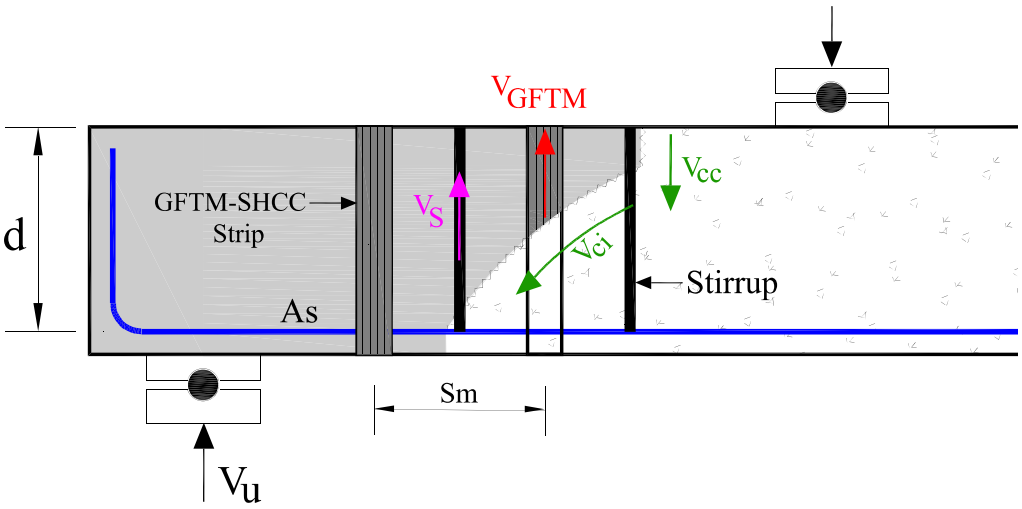


Fig.13. Mechanical model for RC beams strengthened with GFTM-SHCC strips.

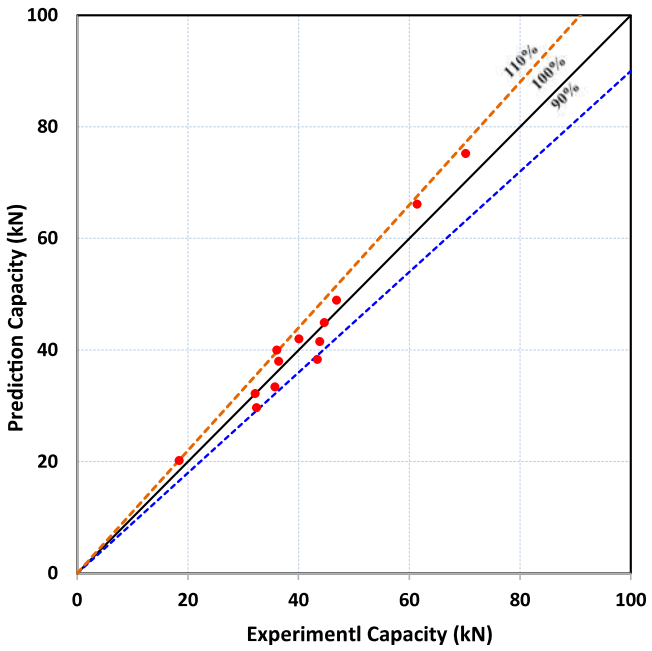


Fig.14. Prediction capacities versus Experimental results.

strains for all tested specimens were plotted in Fig. 12. The developed shear stresses for all RC beams were consistent with the recorded shear loads. Values of the shear strains displayed that all RC beams, without web reinforcements in the shear zone but strengthened in shear using GFTM-SHCC strips, except specimens $BT_{2\text{-}150\text{-}UW\text{-}90}$ and $BT_{4\text{-}225\text{-}UW\text{-}90}$, exhibited higher shear strains at failure with respect to the corresponding control RC beam BC1. It could be attributed to the $BT_{2\text{-}150\text{-}UW\text{-}90}$ specimen's insufficient number of GFTM layers within the SHCC strips and the $BT_{4\text{-}225\text{-}UW\text{-}90}$ specimen's poor interaction between the concrete substrate and the strengthening material due to the higher spacing between the SHCC strips. The shear strains at failure of BC1, $BT_{2\text{-}150\text{-}UW\text{-}90}$, and $BT_{4\text{-}225\text{-}UW\text{-}90}$ were 4093, 1752, and 3915 μmm/mm, respectively. Except for the above-mentioned RC beams, the values of the shear strains at failure for the rest of the specimens were in the range of 6214–10897 μmm/mm as shown in Table 8. Moreover, strengthened specimens $BT_{4\text{-}150\text{-}UW\text{-}90\text{-}H1}$ and $BT_{4\text{-}150\text{-}UW\text{-}90\text{-}H2}$, with aligned or unaligned GFTM-SHCC strips relative to the internal stirrups, demonstrated a significant efficiency and were able to decrease the shear strains compared to the reference beam BC2 at the same load levels. The developed shear strains for $BT_{4\text{-}150\text{-}UW\text{-}90\text{-}H1}$ and $BT_{4\text{-}150\text{-}UW\text{-}90\text{-}H2}$ RC beams decreased by approximately 48% and 22%, respectively, compared to the reference specimen BC2.

4. Theoretical analysis

4.1. *A simple model for estimating the ultimate shear capacities (V_{uth})*

Based on the mechanical model adopted in Fig. 13, the ultimate shear capacity (V_{uth}) of all tested RC beams can be determined by summation of the shear capacities of concrete (V_{crth}), web reinforcements (V_s) and gain of GFTM-SHCC strips (V_{GFTM}), as given in Eq. (2).

$$V_{uth} = V_{crth} + V_s + V_{GFTM} \tag{2}$$

The shear capacity of concrete was calculated based on ACI 318–19 [48] by summation of the shear carried by the aggregate interlock (V_{ci}), concrete in compression zone (V_{cc}), and dowel action of longitudinal reinforcement (V_{cd}), as given by Eq. (3).

$$V_{crth} = \left[0.16\lambda\sqrt{f_c^{'}} + 17\rho\left(\frac{V.d}{M}\right)\right]b.d \tag{3}$$

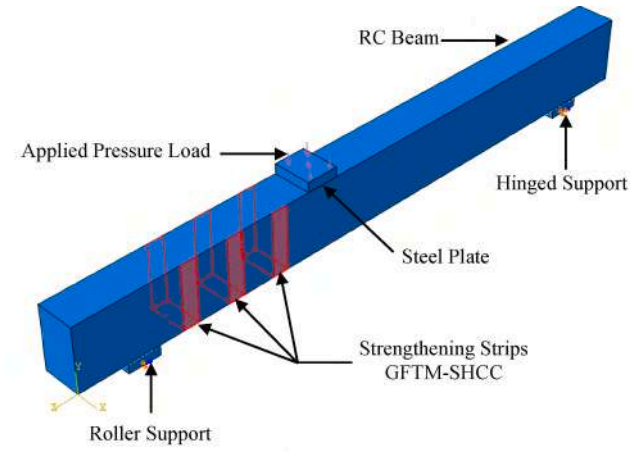
where λ is a concrete parameter equal to 1.00 for the normal weight concrete; $f_c^{'}$ is concrete compressive cylinder strength; ρ is the longitudinal reinforcement ratio, V is the shear force at the considered section and M is the corresponding moment at that section. For simplicity, the value of M/V can be replaced by the shear span (a); see Eq. (4).

$$V_{crth} = \left[0.16\lambda\sqrt{f_c^{'}} + 17\rho\left(\frac{d}{a}\right)\right]b.d \tag{4}$$

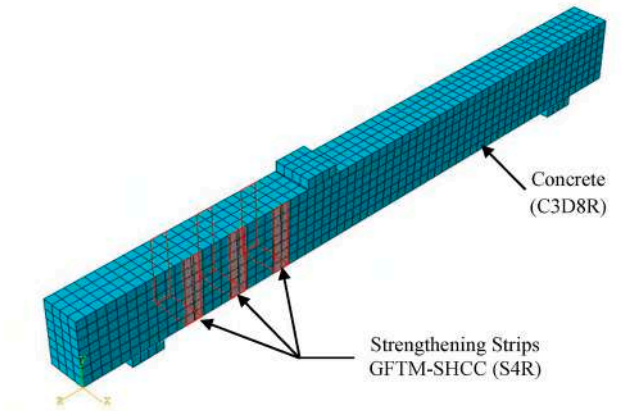
The shear capacity of vertical web reinforcements (V_s) can be calculated by Eq. (5).

$$V_S = A_w \times f_{yw} \times \frac{d}{s_w} \tag{5}$$

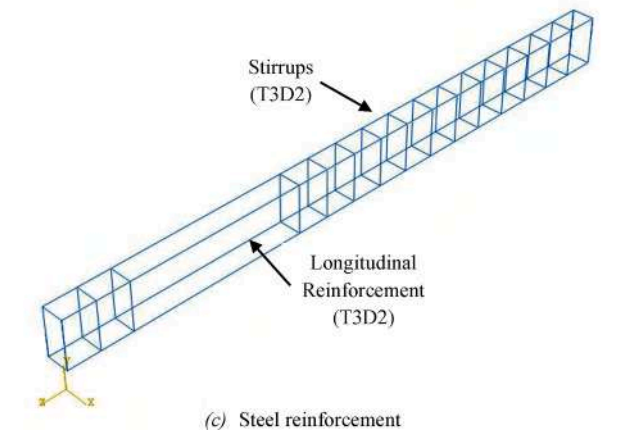
where A_w is the total area of web reinforcements, f_{yw} is the tensile yield strength of the used web reinforcements, d is the effective depth of the section, s_w is the longitudinal spacing between stirrups. The shear capacity of GFTM-SHCC strips (V_{GFTM}) is the sum of capacities for plain SHCC strip and the embedded fiber mesh in SHCC strip, as presented in Eq. (6).



(a) Assembly of RC beam strengthened with U-wrapped GFTM-SHCC strips



(b) Generated mesh.



(c) Steel reinforcement

Fig. 15. Finite element modeling of strengthened RC beam [50].

$$V_{GFTM} = k_j k_a \left[\left(A_{SHCC} \times f_{tyi} + A_f \times f_f \right) \times sin\alpha \times \frac{d}{s_m} \right] \quad (6)$$

where A_{SHCC} is the total cross-sectional area of plain SHCC strips; f_{tyi} is the tensile stress of SHCC matrix at yield point which can be calculated according to JSCE [49] as$f_{tyi} = f_{ti}/\gamma_c$, f_{ti} is the ultimate tensile strength of SHCC matrix and γ_c is the material strength factor = 1.30, A_f is the total nominal area of fiber per strip width; f_f is the tensile strength of the used fiber, s_m is the longitudinal spacing between strips (center to center). kj considers the effect of the jacket configurations and equal 0.55 for two side-bonded strips, 1.00 for U-wrapped strips, and 1.05 for fully wrapped strips. In addition, ka represents the effect of the location of the strengthening strips relative to the internal stirrups and equal 1.00 in case of the strengthening strip is aligned with the internal stirrups and 1.35 in case of the strengthening strip is un-aligned with the internal stirrups.

4.2. Verification of the proposed ultimate shear capacity formula against the experimental results

To verify the accuracy of the proposed equation for ultimate shear capacities (V_{uth}), the experimental shear resistances for the tested specimens were compared with those obtained from the proposed equation considering all studied parameters as graphed in Fig. 14. It can be observed that the proposed equation gives satisfactory shear capacities considering almost test parameters. In addition, the variation in results of the proposed equation ranged between 3% and 19% and the coefficient of variation (COV) was about 10%.

5. Numerical analysis

A three-dimensional (3D) non-linear finite element model (FEM) was constructed using ABAQUS software [50] and then verified against the experimental records. The goal of the numerical analysis was to provide reliable predictions of the shear performance of RC beams strengthened using intermittent or continuous GFTM-SHCC strips.

5.1. Finite element modeling

In the current model, eight-node (every node has three degrees of freedom in translation) linear brick reduced integration hourglass control solid elements (C3D8R) were defined to model concrete and steel plates. On the other hand, the GFTM-SHCC strengthening strips were simulated by using four-node doubly curved reduced integration hourglass control finite membrane strains shell elements (S4R) as depicted in Fig. 15. Moreover, both longitudinal reinforcements and shear stirrups were modelled using 2-node linear 3D truss elements (T3D2) with an axial-only stiffness.

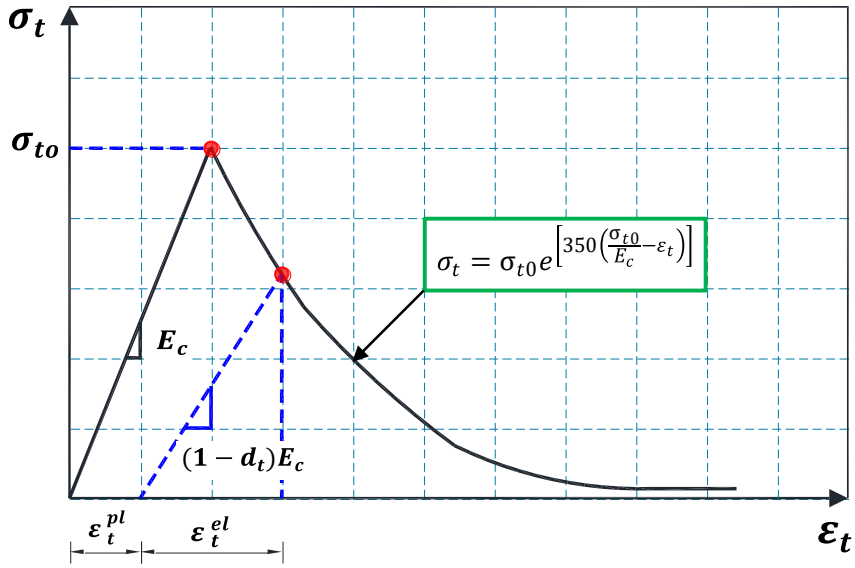
In order to define the softening behavior of concrete and strain-hardening responses of SHCC materials, the concrete damage plasticity model (CDPM) was utilized to simulate both concrete and GFTM-SHCC strip elements. Two principal characteristics, compressive crushing and tensile cracking of concrete and SHCC, were required to construct the CDPM [50].

The tensile uniaxial response of concrete is shown in Fig. 16(a). Until the failure stress, σ_{to}, is reached, the tensile stress strain behavior follows a linear response. Micro-cracks emerge beyond the failure stress as the tensile stress–strain response softens. Moreover, the compressive stress–strain response is represented in Fig. 16(b). Until the value of the initial yield stress, σ_{co}, the behavior was linear. After the initial yield stress, the stress strain followed a stress-hardening pattern until it reached the value of the compressive ultimate stress, σ_{cu}. Beyond the compressive ultimate stress, the compressive stress–strain behavior indicated stress softening. As shown in Eqs. (7) and (8), ABAQUS can automatically transform user-supplied uniaxial stress-inelastic strain curves to stress versus plastic-strain curves.

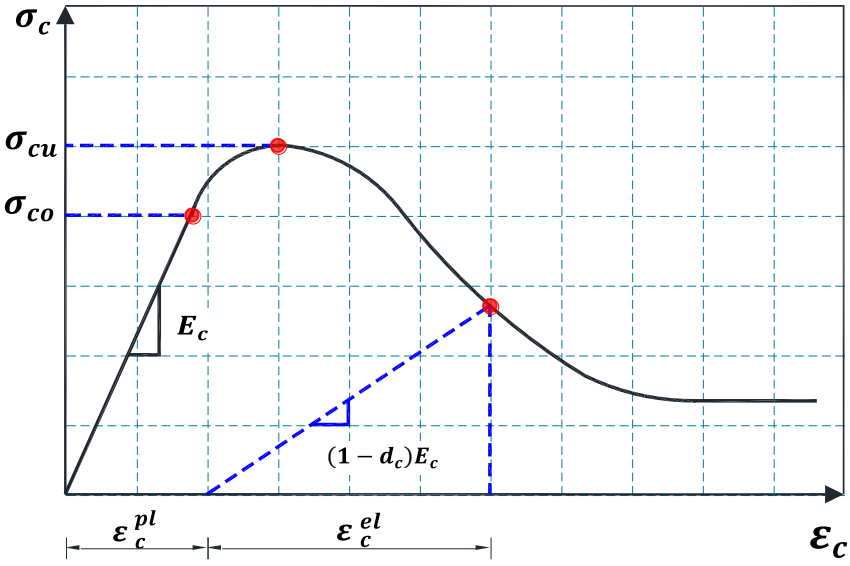
$$\sigma_t = \sigma_t\left(\varepsilon_t^{pl}, \varepsilon_t^{\cdot pl}\right) \quad (7)$$

$$\sigma_c = \sigma_c\left(\varepsilon_c^{pl}, \varepsilon_c^{\cdot pl}\right) \quad (8)$$

where the subscripts t and c stand for tension and compression, respectively. σ_t and σ_c represent the concrete's tensile and compressive stresses, respectively. ε_t^{pl} and ε_c^{pl} are the equivalents plastic strains



(a) Uniaxial tensile stress-strain response for concrete.



(b) Uniaxial compressive stress-strain responses for both concrete and GFTM-SHCC strips.

Fig. 16. Uniaxial compressive and tensile stress–strain responses [50].

Table 9
The CDPM parameters.

Dilation angle	Eccentricity	f_{b0}/f_{c0}	K	Viscosity parameter
20	0.1	1.16	0.667	0

f_{b0}: is the equiaxial compressive yielding stress,f_{c0}: is the uniaxial compressive yielding stress,K: is the shape coefficient.

while $\dot{\varepsilon}_t^{pl}$ and $\dot{\varepsilon}_c^{pl}$ are the equivalents plastic strain rates.

As demonstrated in Eqs. (9) and (10), the failure mechanisms for both concrete and SHCC material under tension and compression loadings were inserted using the compressive and tensile damage parameter formulas recommended by Birtel and Mark [51].

$$d_t = 1 - \frac{\sigma_t E_c^{-1}}{\varepsilon_t^{pl}(1/b_t - 1) + \sigma_t E_c^{-1}} \tag{9}$$

$$d_c = 1 - \frac{\sigma_c E_c^{-1}}{\varepsilon_c^{pl}(1/b_c - 1) + \sigma_c E_c^{-1}} \tag{10}$$

where d_t and d_c represent the tensile and compressive damage parameters, respectively. ε_t^{pl} and ε_c^{pl} refer to the plastic strains corresponding to the tensile and compressive stresses, respectively. b_t and b_c are constant parameters in the range from 0 to 1.

The Sanez model [52] was used to calculate the uniaxial compressive stress–strain behavior for concrete and SHCC materials by means of Eqs. (11) to (16).

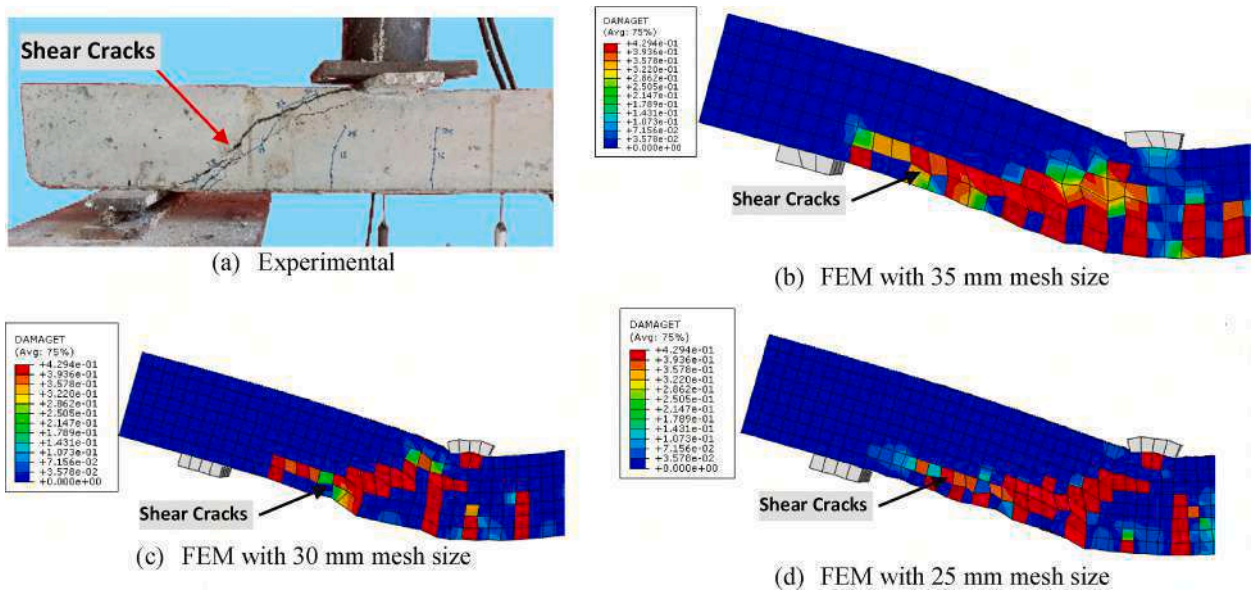


Fig. 17. Experimental failure pattern versus FEM with various mesh sizes at failure load for BC1 specimen.

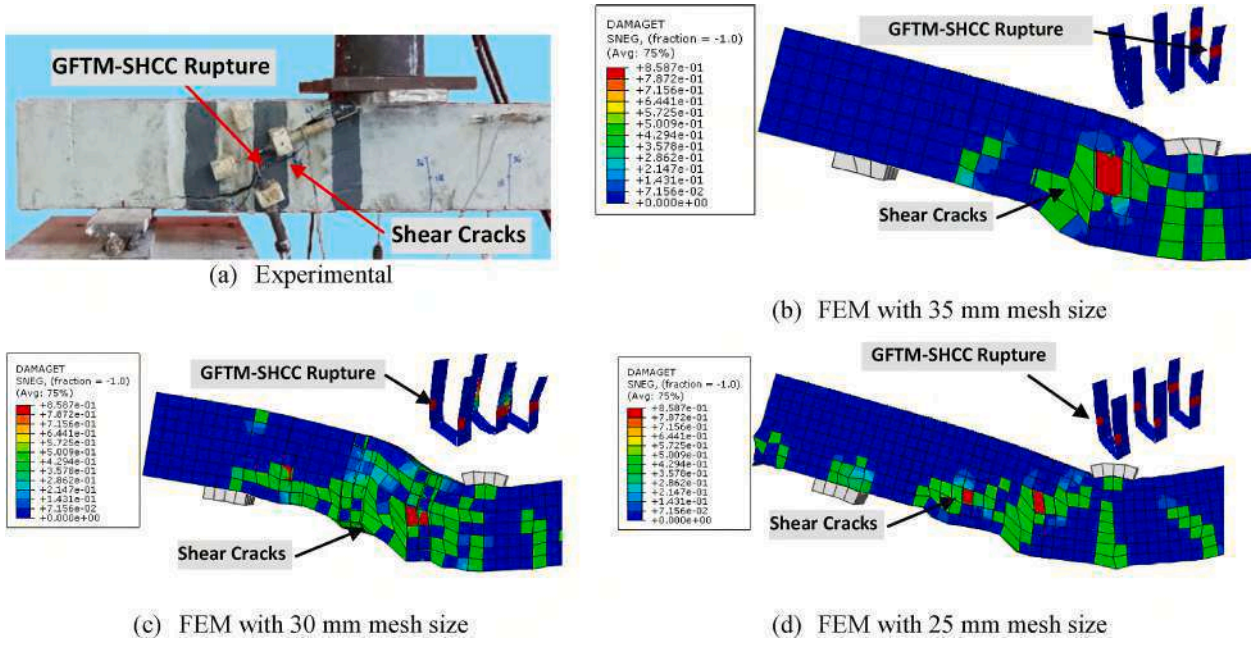


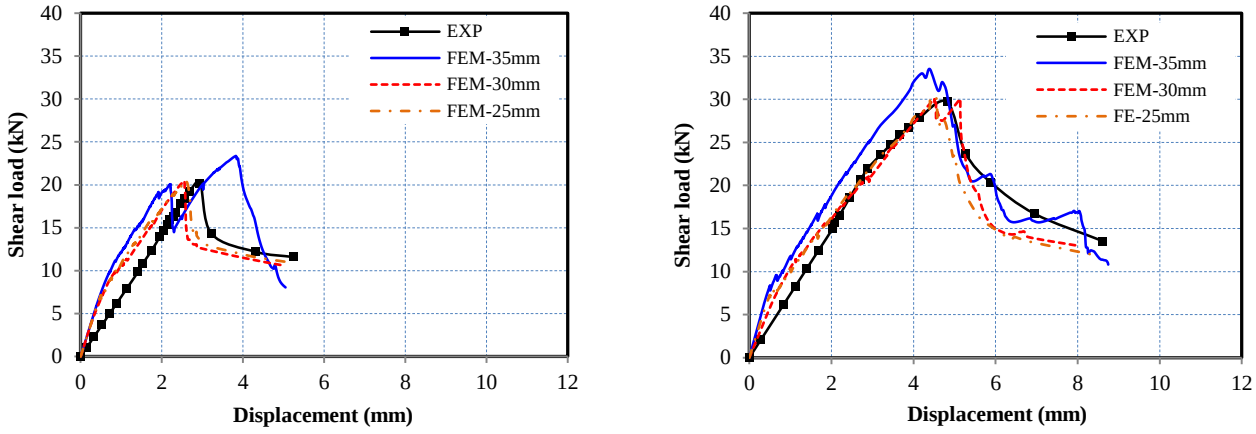
Fig. 18. Experimental failure pattern versus FEM with various mesh sizes at failure load for $BT_{2\text{-}150\text{-}UW\text{-}90}$ specimen.

Table 10
Experimental versus finite element load–deflection responses for BC1 and $BT_{2\text{-}150\text{-}UW\text{-}90}$ specimens.

Specimen	Ultimate shear capacity (kN)				Maximum mid-span deflection (mm)				Failure mode			
	Experimental capacity (kN)	Numerical capacity (kN)			Experimental Deflection (mm)	Numerical Deflection (mm)			Experimental Failure mode	Numerical Failure mode		
		Mesh size (mm)				Mesh size (mm)				Mesh size (mm)		
		35	30	25		35	30	25		35	30	25
BC1	20.2	23.4	20.5	20.5	5.26	5.05	5.01	5.1	S	S	S	S
$BT_{2\text{-}150\text{-}UW\text{-}90}$	29.7	33.5	30.1	30.3	8.62	8.75	8.02	8.32	SR	SR	SR	SR

$$\sigma_c = \frac{E_c \varepsilon_c}{1 + (R + R_E - 2)\left(\frac{\varepsilon_c}{\varepsilon_0}\right) - (2R - 1)\left(\frac{\varepsilon_c}{\varepsilon_0}\right)^2 + R\left(\frac{\varepsilon_c}{\varepsilon_0}\right)^3} \quad (11)$$

$$E_c = 4700\sqrt{\sigma_{cu}} \quad (12)$$



(a) BC1 (b) $BT_{2\text{-}150\text{-}UW\text{-}90}$

Fig. 19. Comparison between experimental and finite element load-mid span deflection behaviors.

Table 11
Model size and job time.

Specimen	Number of elements			Number of degrees of freedom (DOF)			CPU time (minutes)		
	Mesh size (mm)			Mesh size (mm)			Mesh size (mm)		
	35	30	25	35	30	25	35	30	25
BC1	1851	2424	3884	7791	10,122	15,546	95	137	423
$BT_{2\text{-}150\text{-}UW\text{-}90}$	1896	2532	4010	8439	11,256	16,842	129	186	497

$$R = \frac{R_E}{3} - 0.25 \quad (13)$$

$$R_E = \frac{E_c}{E_0} \quad (14)$$

$$E_0 = \frac{\sigma_{cu}}{\varepsilon_0} \quad (15)$$

$$\varepsilon_0 = 0.0025 \quad (16)$$

where E_c is the elastic modulus and is estimated according to the ACI 318–19 [48] in MPa, ε_c is the compressive strain corresponding to the compressive strength,σ_c, and σ_{cu} is the maximum compressive strength of concrete/SHCC in MPa. Evaluation of the rest parameters R, R_E, E_0, and ε_0 are performed by Eqs. (13) to (16), respectively, as reported in [53].

The uniaxial tensile stress–strain behaviors for concrete and GFTM-SHCC strips were modelled in two stages; a linear response followed by a softening branch for concrete and a strain-hardening response in the case of GFTM-SHCC strips. To model the linear part of each material, the elastic modulus (E_c) and the tensile strength (σ_{t0}) were mandatory. According to Eq. (12), E_c was 23,500 and 42038 MPa for concrete and SHCC, respectively. Furthermore, the tensile softening branch was calculated based on the recommendations of Ganganagoudar et al. [54] using Eq. (17) as shown in Fig. 16(a), while the strain-hardening response was modelled as experimentally recorded (Fig. 2). A Poissons' ratio of 0.2 was set for concrete and SHCC, while the plasticity parameters recommended by Mansour [55] and listed in Table 9 were defined for the CDPM.

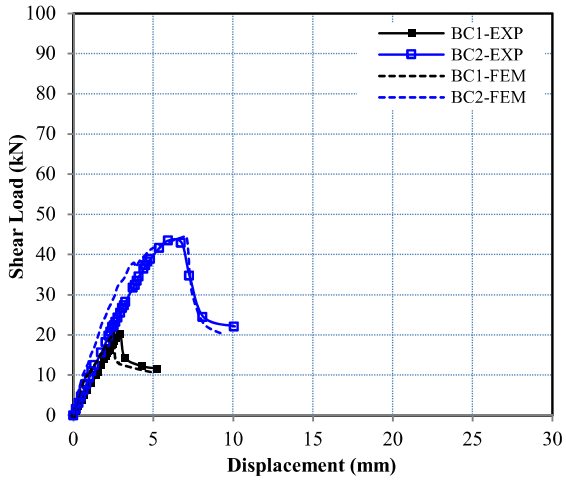
$$\sigma_t = \sigma_{t0} e^{\left[350\left(\frac{\sigma_{t0}}{E_c} - \varepsilon_t\right)\right]} \quad (17)$$

where ε_t is the tensile strain corresponding to the tensile strengthσ_t..

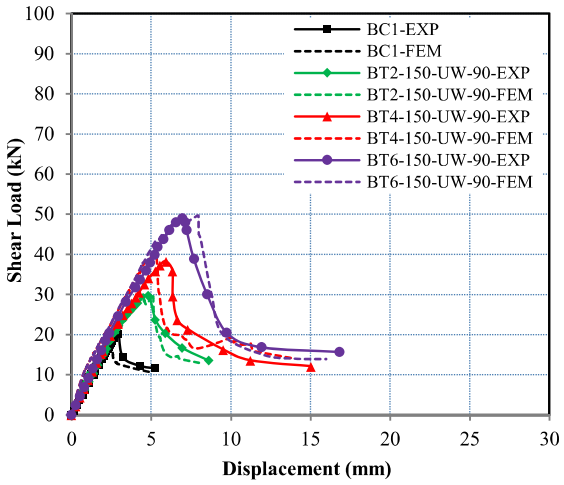
On one hand, the steel reinforcement in the case of shear failure was modelled using an elastic-perfectly plastic response with identical characteristics in tension and compression. The elstic-perfectly plastic model could be suggested when the ultimate axial loads reached in the steel bars were lower or close to the yield load. On the other hand, for flexure failure accompained by steel yielding, the steel reinforcement was modelled using elastic–plastic model with strain hardening. The Poisson's ratio and the elastic modulus of the steel were 0.3 and 200 GPa, respectively, while the yield stress was defined based on experiments (Table 4). Because of indentations and sufficient development lengths, the steel reinforcement did not slip from the RC beam, and therefore was modelled as fully bonded using the embedded region method.

Due to the variation in strengthening schemes and reinforcement details, especially shear stirrups along the span of the RC beams, entire beams either control or strengthened using GFTM-SHCC strips were numerically modelled according to the dimensions and geometries shown in Fig. 4 and Table 5. Experimental records demonstrated that no debonding/separation was observed between the GFTM-SHCC strengthening strips and the substrate RC beams, consequently a perfect bond interaction was used to link the two surfaces using tie constraint. In order to prevent local failure in concrete due to concentration of stresses, 30 mm steel plates were positioned at the loading point and the two end supports, and the load was implemented as pressure with a loading rate of 0.3% of the applied total load. The boundary conditions consisted of two supports; the right one was restrained against displacements along the X, Y, and Z axis and rotation about the Z-axis (hinged support), while the left support was roller and restrained against displacements along the X and Y axis and rotation about the Z-axis. The model was stopped at the ultimate mid-span deflection experimentally recorded.

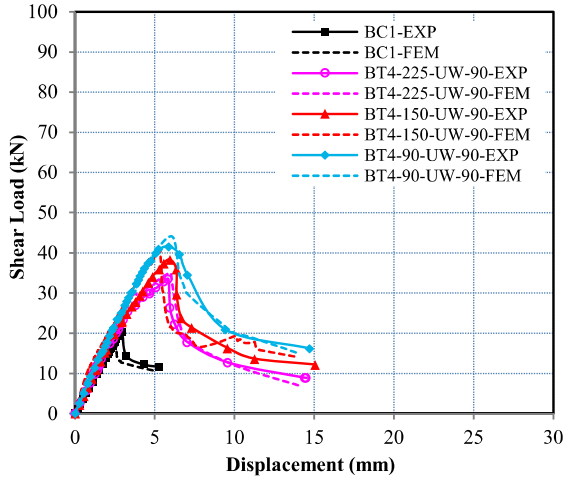
In the current study, a mesh sensitivity analysis was performed using three alternative element sizes of 35, 30, and 25 mm in order to identify the ideal mesh size for the numerical analysis. Fig. 17 and Fig. 18 show the effect of the proposed mesh sizes on the failure patterns of specimens BC1 and $BT_{2\text{-}150\text{-}UW\text{-}90}$, respectively. For the control specimen BC1, all



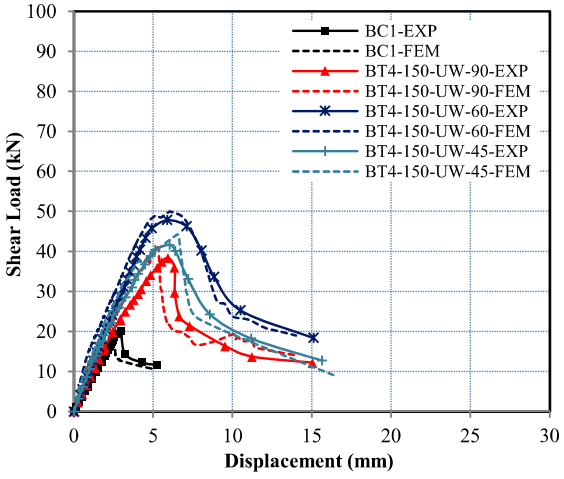
(a) Control specimens



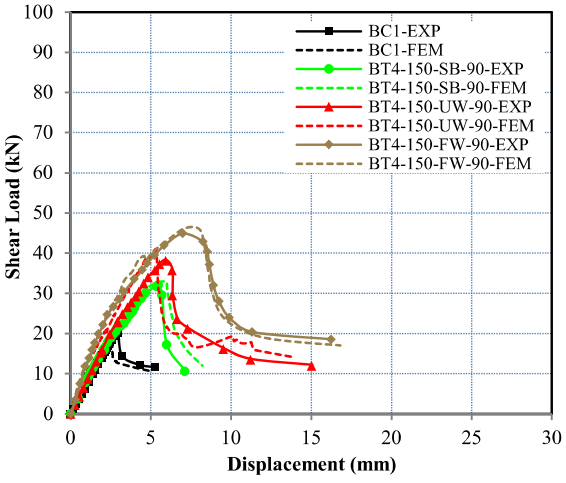
(b) Effect of number of GFTM layers within the SHCC strip



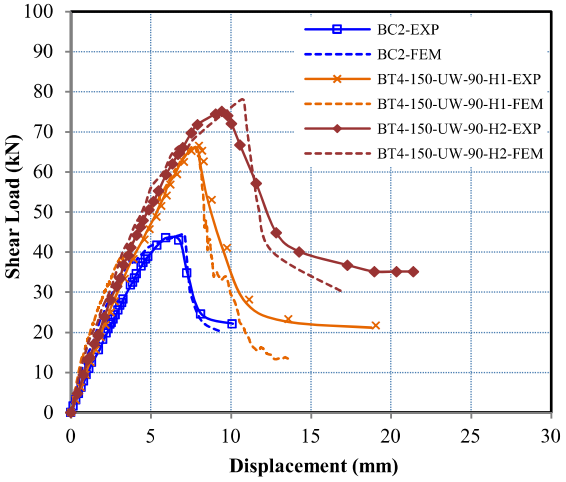
(c) Effect of spacing between GFTM-SHCC strips



(d) Effect of orientation angle of GFTM-SHCC strips



(e) Effect of GFTM-SHCC configuration



(f) Effect of the location of GFTM-SHCC strips relative to the internal stirrups

Fig. 20. Experimental versus numerical load mid-span deflection responses for different parameters.

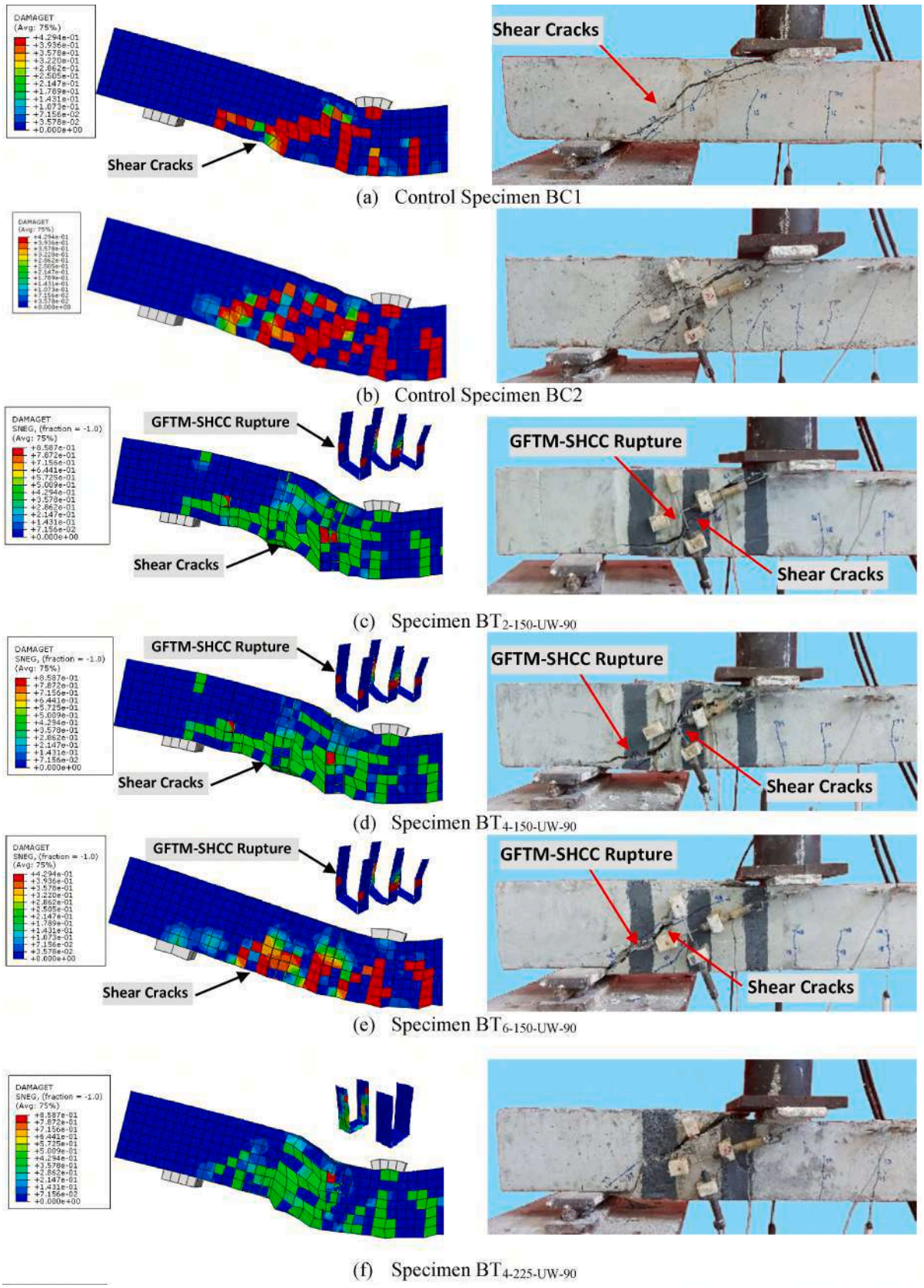
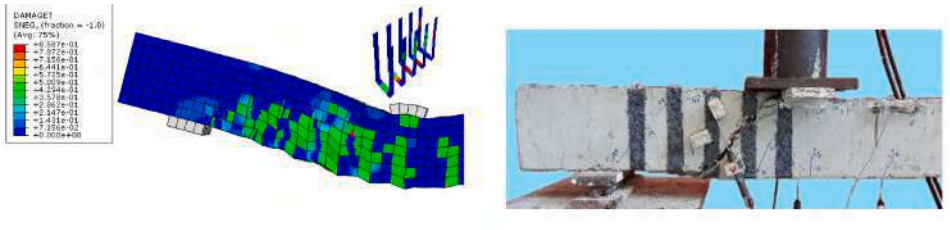
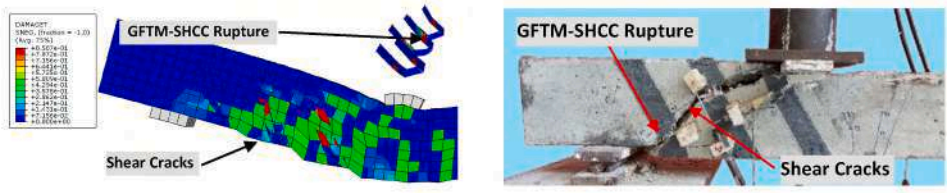


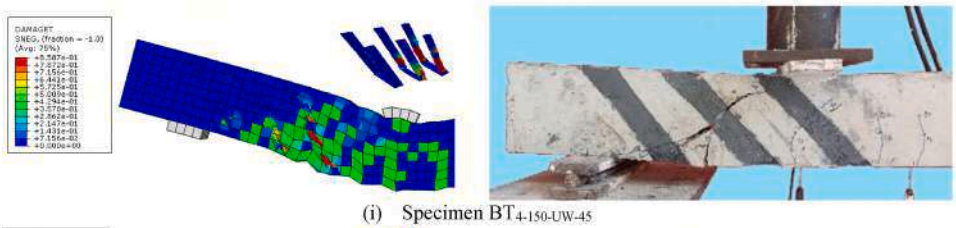
Fig. 21. Experimental versus numerical failure patterns at ultimate load for selected specimens.



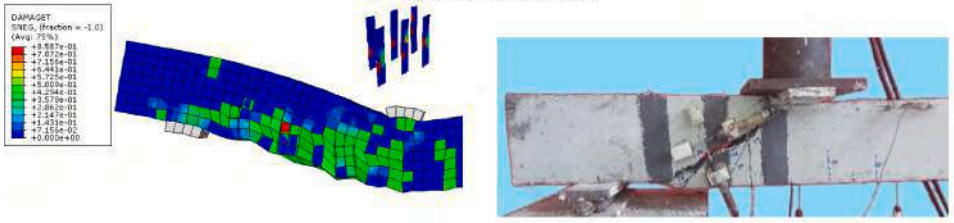
(g) Specimen $BT_{4\text{-}90\text{-}UW\text{-}90}$



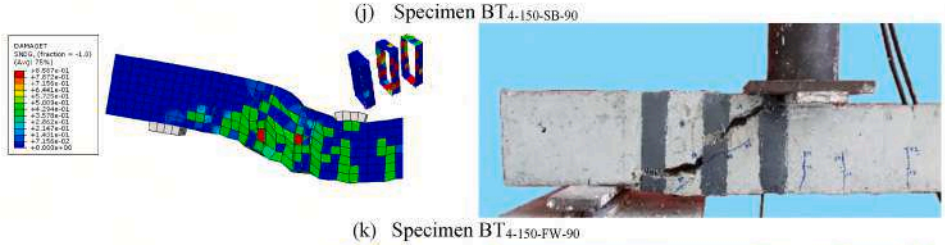
(h) Specimen $BT_{4\text{-}150\text{-}UW\text{-}60}$



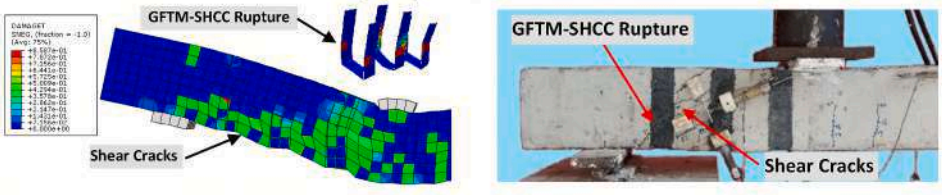
(i) Specimen $BT_{4\text{-}150\text{-}UW\text{-}45}$



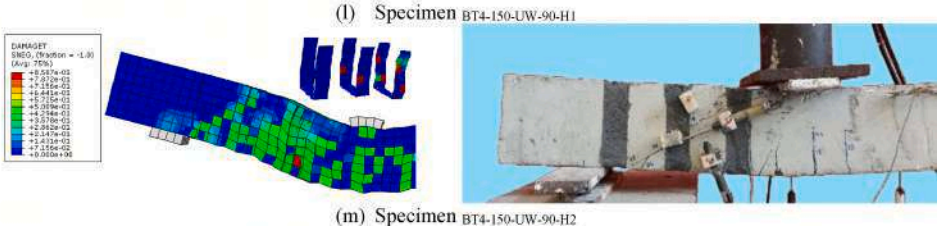
(j) Specimen $BT_{4\text{-}150\text{-}SB\text{-}90}$



(k) Specimen $BT_{4\text{-}150\text{-}FW\text{-}90}$



(l) Specimen $BT4\text{-}150\text{-}UW\text{-}90\text{-}H1$



(m) Specimen $BT4\text{-}150\text{-}UW\text{-}90\text{-}H2$

Fig. 21. (*continued*).

mesh sizes succeeded in capturing the major shear crack that was experimentally recorded. As the number of parts and the complexity of the structure increase, such as in strengthened beams, the impact of mesh size on failure pattern becomes more obvious. Although the various mesh sizes were successful in predicting shear cracks in the $BT_{2\text{-}150\text{-}UW\text{-}90}$ specimen, the mesh size of 35 mm failed to catch the rupture of

Table 12
Experimental versus numerical results.

Specimen	Ultimate shear capacity (kN)			Maximum mid-span deflection (mm)		
	Experimental ($V_{u,\ EXP}$)	Numerical ($V_{u,\ FE}$)	$V_{u,\ FE}$ / $V_{u,\ Exp}$	Experimental ($\Delta_{max,\ EXP}$)	Numerical ($\Delta_{max,\ FE}$)	$\Delta_{max,\ FE}$ / $\Delta_{max,\ EXP}$
BC1	20.2	20.5	1.01	5.26	5.01	0.95
BC2	43.5	44.5	1.02	10.12	9.50	0.94
$BT_{2\text{-}150\text{-}UW\text{-}90}$	29.7	30.1	1.01	8.62	8.02	0.93
$BT_{4\text{-}150\text{-}UW\text{-}90}$	38.3	41.0	1.07	15.07	14.10	0.94
$BT_{6\text{-}150\text{-}UW\text{-}90}$	48.9	49.7	1.02	16.85	16.13	0.96
$BT_{4\text{-}225\text{-}UW\text{-}90}$	33.4	35.0	1.05	14.51	14.00	0.96
$BT_{4\text{-}90\text{-}UW\text{-}90}$	41.5	44.0	1.06	14.72	14.18	0.96
$BT_{4\text{-}150\text{-}UW\text{-}60}$	47.8	49.9	1.04	15.12	14.26	0.94
$BT_{4\text{-}150\text{-}UW\text{-}45}$	41.6	44.1	1.06	15.63	16.50	1.06
$BT_{4\text{-}150\text{-}SB\text{-}90}$	32.2	33.0	1.02	7.11	7.85	1.10
$BT_{4\text{-}150\text{-}FW\text{-}90}$	44.9	46.1	1.03	16.22	16.80	1.04
$BT_{4\text{-}150\text{-}UW\text{-}90\text{-}H1}$	66.1	66.5	1.01	18.78	19.40	1.03
$BT_{4\text{-}150\text{-}UW\text{-}90\text{-}H2}$	75.2	78.0	1.04	21.37	21.56	1.01
Average			1.03			0.99
Standard deviation			0.021			0.055
Coefficient of variation (COV)%			2.03%			5.61%

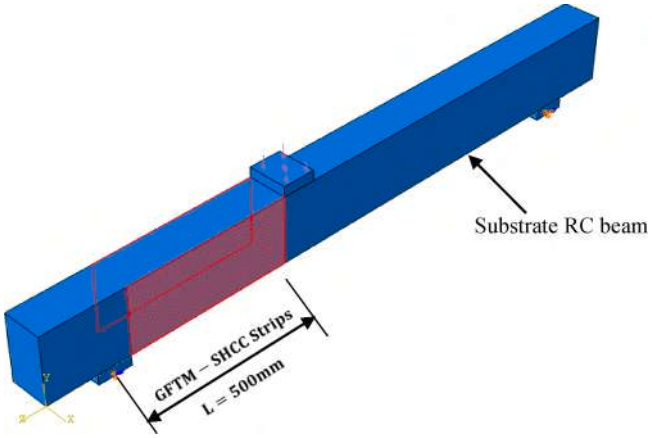


Fig. 22. RC beams strengthened by using side-bonded GFTM-SHCC strips along the whole length of the critical shear span.

all SHCC strips.

The results in Table 10 and Fig. 19 show that numerical models with a mesh size of 35 mm were unable to predict the experimental failure load with high accuracy, in contrast to smaller mesh sizes of 30 mm or 25 mm. On one hand, the experimental ultimate load of the control specimen BC1 was 20.2 kN, while the numerical ultimate loads were 23.4, 20.5, and 20.5 kN for mesh sizes of 35, 30, and 25 mm, respectively. On the other hand, the strengthened specimen $BT_{2\text{-}150\text{-}UW\text{-}90}$ failed at 29.7 kN, whereas the finite element predictions were 33.5, 30.1, and 30.3 kN for mesh sizes of 35, 30, and 25 mm, respectively. Moreover, all of the proposed mesh sizes well captured the maximum mid-span deflection for both control and strengthened beams with respect to the experimental findings.

Despite that, reducing the mesh size to less than 30 mm had no significant effect on the shear performance of the analyzed specimens, but it significantly increased the required computational time as listed in Table 11. Consequently, a mesh size of 30 mm was set for the finite element modeling to achieve a good balance between the numerical efficiency and the job-time.

Table 13
Numerical results of RC beams strengthened using continuous GFTM-SHCC strips.

Group No.	Specimen	Shear capacities (kN)			Mid-span deflections (mm)		Ductility		Failure mode
		Yielding (V_y)	Ultimate (V_u)	Capacity Gain %	Yielding Δ_y	Maximum $\Delta_{max.}$	Index $\Delta_{max.}/\Delta_y$	Ductility Gain %	
Control	BC1	20.1	20.5	NA	3.62	5.01	1.38	NA	S
	BC2	42.2	44.5	NA	5.70	9.50	1.67	NA	S
1	$BT_{2\text{-}SB\text{-}90}$	33.7	35.4	73	5.03	8.10	1.61	17	SR
	$BT_{4\text{-}SB\text{-}90}$	40.8	43.8	114	5.94	10.30	1.73	25	SR
	$BT_{6\text{–}SB\text{-}90}$	46.9	50.7	147	6.54	11.92	1.82	32	SR
	$BT_{2\text{-}UW\text{-}90}$	40.2	42.3	106	6.03	9.84	1.63	18	SR
	$BT_{4\text{-}UW\text{-}90}$	51.6	54.2	164	5.40	15.22	2.82	104	SR
	$BT_{6\text{-}UW\text{-}90}$	56.8	67.9	231	8.82	19.35	2.19	59	SR
	$BT_{2\text{-}FW\text{-}90}$	42.5	50.1	144	6.39	16.39	2.56	85	SR
	$BT_{4\text{-}FW\text{-}90}$	53.6	63.5	210	4.69	18.02	3.84	178	SR
	$BT_{6\text{-}FW\text{-}90}$	66.3	78.6	283	5.47	20.18	3.68	167	SR
2	$BT_{2\text{-}SB\text{-}90\text{-}H}$	54.7	58.6	32*	4.31	13.41	3.11	86*	SR
	$BT_{4\text{-}SB\text{-}90\text{-}H}$	67.2	72.5	63*	5.55	17.75	3.20	92*	SR
	$BT_{6\text{-}SB\text{-}90\text{-}H}$	78.6	84.9	91*	6.18	20.54	3.32	99*	SR
	$BT_{2\text{-}UW\text{-}90\text{-}H}$	84.8	89.3	101*	5.02	16.29	3.25	95*	SR
	$BT_{4\text{-}UW\text{-}90\text{-}H}$	90.3	95.4	114*	7.43	25.26	3.40	104*	SR
	$BT_{6\text{-}UW\text{-}90\text{-}H}$	99.9	118.7	167*	5.39	30.00	5.57	234*	SFY
	$BT_{2\text{-}FW\text{-}90\text{-}H}$	77.4	91.2	105*	5.65	26.93	4.77	186*	SR
	$BT_{4\text{-}FW\text{-}90\text{-}H}$	98.9	117.2	163*	4.35	30.00	6.90	313*	SFY
	$BT_{6\text{-}FW\text{-}90\text{-}H}$	101.2	119.9	169*	4.34	30.00	6.91	314*	SFY

* The values were calculated with respect to the control specimen (BC2).
S: Shear failure due to major shear crack, SR: Shear failure accompanied with SHCC rupture, SFY: Shear-flexural cracks.

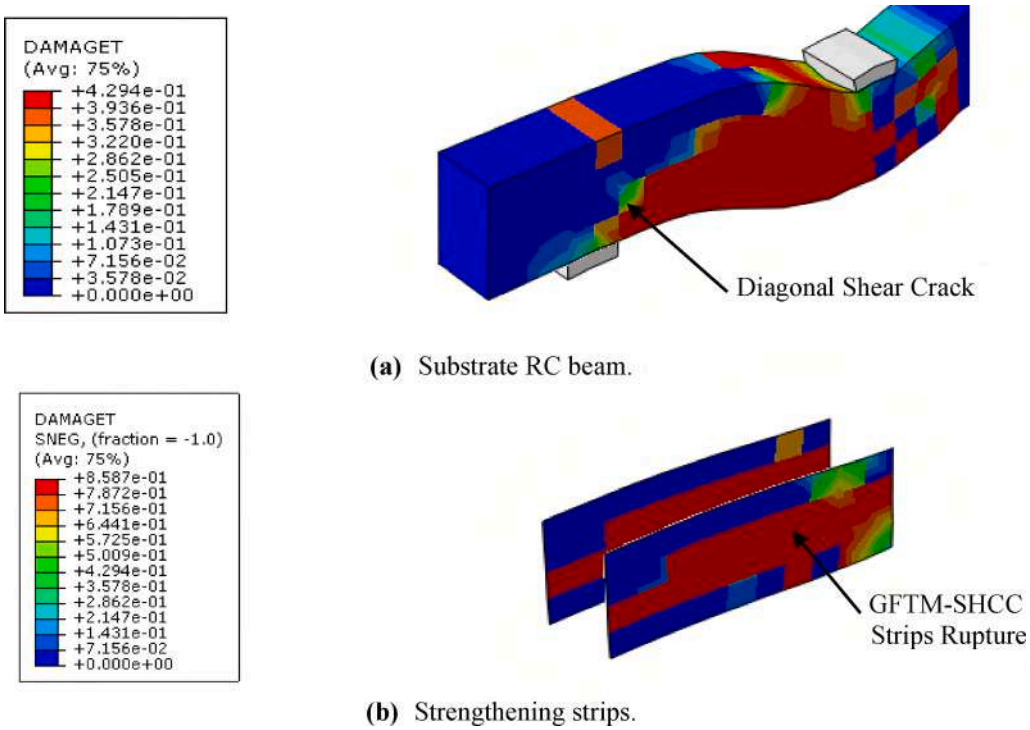


Fig. 23. Shear failure and GFTM-SHCC rupture of $BT_{2\text{-}SB\text{-}90}$ specimen in group No. 1.

5.2. Verification against experimental results

The numerical results were verified against the experimental records in terms of the tensile damage (DAMAGET), shear capacity, and load mid-span defelction response to check the efficiency of the constructed model. A comparison between the experimental and numerical load mid-span deflection behaviors for all test matrix specimens is shown in Fig. 20, while failure patterns of all the specimens with different configurations and orientations are depecited in Fig. 21. It can be noted that the proposed 3D non-linear FEM was efficiently able to predict the load mid-span deflection responses at different loading stages for all RC beams with respect to the experimental records. Additionally, Table 12 shows that the average ratio and the coefficient of variation between the numerical ultimate shear capacities ($V_{u,\ FE}$) and the experimental ones ($V_{u,\ EXP}$) are 1.03 and 2.0%, respectively. Moreover, the average value and the coefficient of variation of the numerical values of the maximum mid-span deflection ($\Delta_{max,\ FE}$) to their experimental records ($\Delta_{max,\ EXP}$) are 0.99 and 5.5%, respectively.

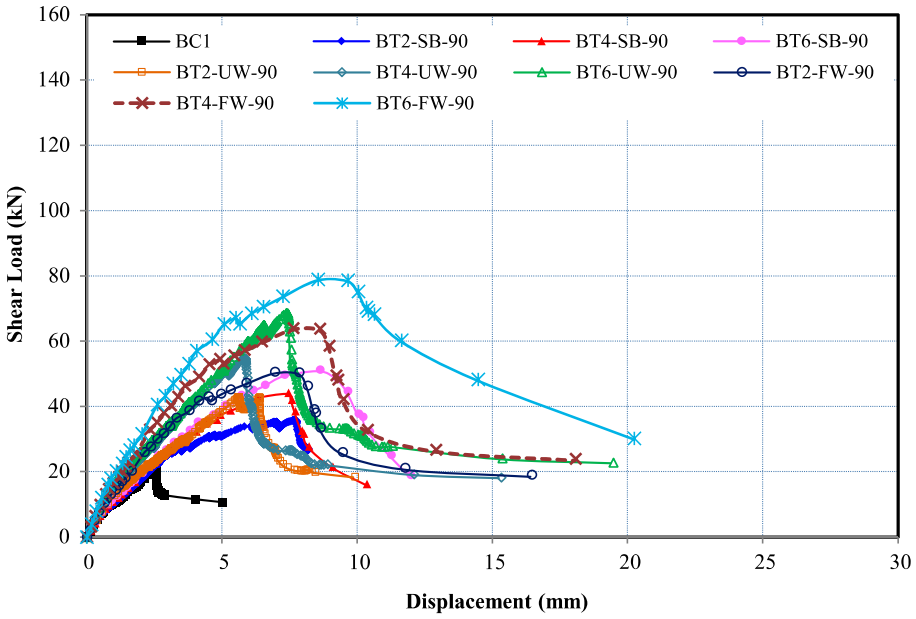
The predicted failure modes for both control and strengthened RC beams agreed with the experimental crack propogations. Fig. 21(a) shows the match between the predicted and the eperimental failure pattern for control beam BC1, where the flexural crack firstly apperaed under the loading point followed by shear failure due to major shear crack within the critical shear span zone. Fig. 21(b) to 21(m) reflect the ability of the numerical model to predict the first flexural crack under load, major and secondary shear cracks within the critical shear region, and the rupture of GFTM-SHCC strengthening strips at failure of selected strengthened RC beams as eperimentally observed.

5.3. Parametric analysis

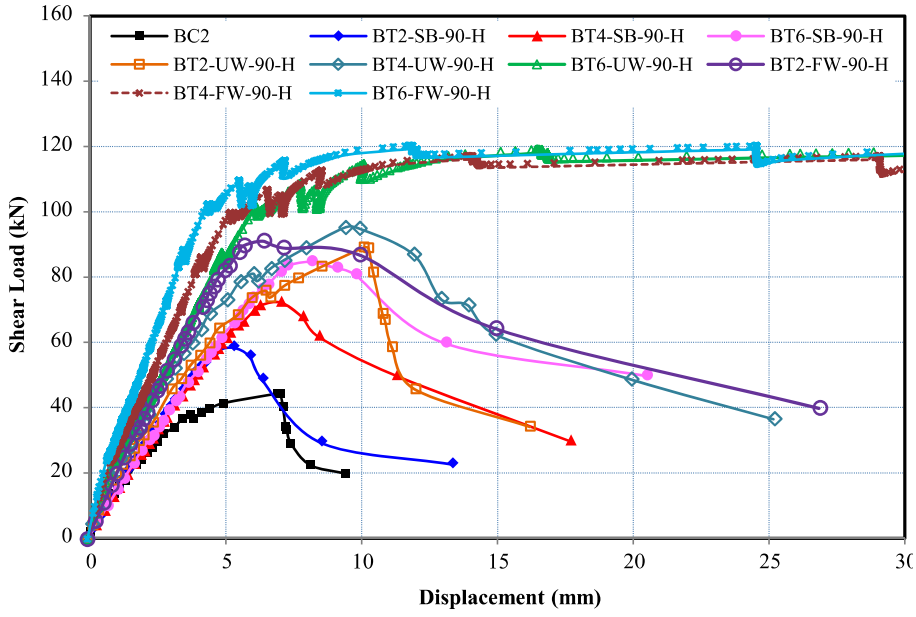
Herein, in this section, the validated model was used to run a parametric study in order to compare the shear performance of RC beams strengthened along the whole length of the critical shear span zone using continuous GFTM-SHCC strips with that of control specimens. The total length of the critical shear span zone was considered as the clear distance between the left support and the loading strip of 500 mm (refer to Fig. 22). Eighteen RC beams strengthened with three different configurations of vertical GFTM-SHCC strips (side-bonded, U-wrapped, or fully-wrapped) reinforced by GFTM layers (2, 4, or 6) within SHCC strengthening strips were suggested. These 18 specimens were divided into two groups: the first (group No. 1) consisted of nine GFTM-SHCC strengthened specimens without internal web reinforcement in the studied shear span, while group No. 2, the same aspects as group No. 1, were strengthened using GFTM-SHCC strips in the presence of internal stirrups. The numerical results of the analyzed two groups, in addition to the control beams BC1 and BC2 are listed in Table 13.

As previously discussed, the control beams showed shear failure mode due to the propagation of shear cracks within the shear zone along the diagonal direction connecting the support and the loading point. Regardless of the strengthening configurations and the number of the GFTM layers within the SHCC strips, at failure load, all RC beams in group No. 1 exhibited shear failure due to the propagation of a major diagonal shear crack accompanied by GFTM-SHCC rupture as shown in Fig. 23. The load mid-span deflection responses for both FE analyzed groups are shown in Fig. 24. With regard to specimens in group No. 1, Fig. 24(a) revealed that the strain of the tensile reinforcment steel did not reach the yielding strain (2100 μmm/mm) as the load suddenly dropped at failure. For this group, as the area of the GFTM-SHCC strengthening strips increased, not only the ultimate shear capacity of RC beams increased but also the slope of the load deflection curves, post the peak, became flatter due to the propogation of shear-flexural cracks instead of shear cracks only at the critical shear zone. Consequently, fully-wrapped strengthened RC beams showed the highest gains in ultimate load and ductility contray to side-bonded strengthened specimens, which did not significantly enhance the shear performance compared to BC1.

It can be noticed that, the strengthenening of RC beams using GFTM-SHCC strips remarkably increased the ultimate capacity and the gain in ductility as compared to BC1, especially when higher layers of GFTM layers were used within the SHCC strengthening strips. Among all the RC beams in group No. 1, specimen $BT_{6\text{-}FW\text{-}90}$ (fully-wrapped with six layers of GFTM within the SHCC strips) recorded the highest gain in both ultimate shear capacity and ductility of 283% and 167%, respectively,



(a) Group No. 1.



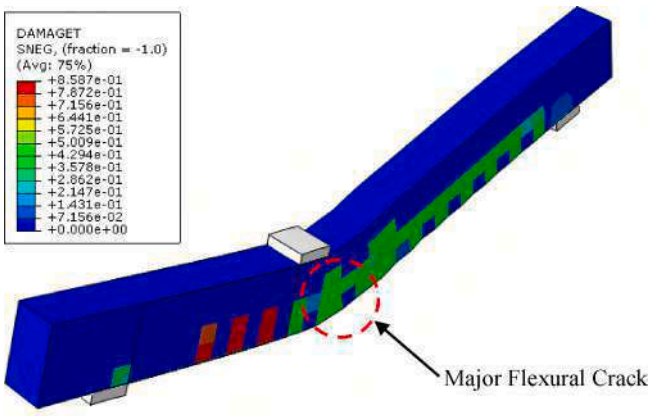
(b) Group No. 2.

Fig. 24. Load mid-span deflection responses for analyzed FE specimens.

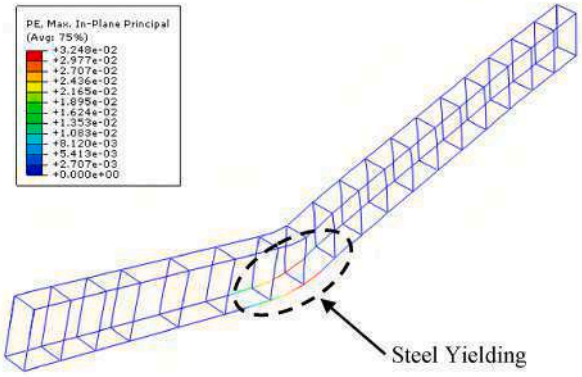
compared to BC1. Additionally, the confinement of the whole critical shear span zone effectively delayed the rupture of the GFTM-SHCC strips and led to a significant increase in the ultimate carrying load capacity and mid-span deflection at failure with respect to intermittent strengthening. The gains in shear capacity and ductility of the continuous strengthened specimen $BT_{4\text{-}FW\text{-}90}$ (the whole shear span was strengthened) were 210% and 178%, respectively, compared to 122% and 172% for the specimen $BT_{4\text{-}150\text{-}FW\text{-}90}$ (intermittent strengthening).

As expected, the lowest gains in shear capacity and ductility among all RC beams in group No. 1 were recorded when side-bonded strips with only two layers of GFTM layers were used. As the number of the GFTM layers within the SHCC strips increased, the shear performance of the analyzed specimens improved. The ultimate shear capacities of specimens $BT_{2\text{-}SB\text{-}90}$, $BT_{4\text{-}SB\text{-}90}$, and $BT_{6\text{-}SB\text{-}90}$ were 35.4, 43.8, and 50.7 kN, respectively, while their gains in ductility were 17, 25, and 32% compared to BC1. On the other hand, the shear capacities of specimens $BT_{2\text{-}UW\text{-}90}$, $BT_{4\text{-}UW\text{-}90}$, and $BT_{6\text{-}UW\text{-}90}$ were 106, 164, and 231% higher than the ultimate load of the control specimen BC1. Although the gain in ductility of U-wrapped strengthened specimens was improved compared to BC1 (the increasing ratio ranged between 18% and 104%), the use of fully-wrapped GFTM-SHCC strips had achieved the highest improvement in ductility among all strengthened specimens in group No. 1 (the gain in ductility ranged between 85% and 178%).

Strengthened RC beams in group No. 2 showed two different failure patterns. All specimens in this group except $BT_{6\text{-}UW\text{-}90\text{-}H}$, $BT_{4\text{-}FW\text{-}90\text{-}H}$, and $BT_{6\text{-}FW\text{-}90\text{-}H}$ exhibited the conventional shear failure associated with GFTM-SHCC rupture without steel yielding. On the contarary, strengthening RC beams either using U-wrapping or fully-wrapping



(a) Flexural cracks.



(b) Tensile reinforcement yielding.

Fig. 25. Flexural failure and steel yielding of $BT_{6\text{-}UW\text{-}90\text{-}H}$ specimen.

techniques completely prevented the propagation of the major shear crack within the critical shear span, especially when six layers of GFTM layers were embedded within the strengthening strips. Consequently, specimens $BT_{6\text{-}UW\text{-}90\text{-}H}$, $BT_{4\text{-}FW\text{-}90\text{-}H}$, and $BT_{6\text{-}FW\text{-}90\text{-}H}$ showed flexural failure due to flexural cracks along the whole length of the RC beams, followed by steel yielding as depicted in Fig. 25. The recorded failure modes explained the superior gain in ductility for U-wrapped and fully-wrapped techniques with respect to side-bonded specimens. Fig. 24(b) shows the sudden decrease of the load after reaching the peak value of side-bonded strengthened specimens, even as a different number of GFTM layers were used, contrary to the high ductility shown by the U-wrapped and fully-wrapped beams ($BT_{6\text{-}UW\text{-}90\text{-}H}$, $BT_{4\text{-}FW\text{-}90\text{-}H}$, and $BT_{6\text{-}FW\text{-}90\text{-}H}$) indicated by the horizontal regions of the load–deflection curves.

Among all the RC beams either experimentally tested (intermittent strengthening) or numerically analyzed (the shear span was fully strengthened), specimens $BT_{6\text{-}UW\text{-}90\text{-}H}$, $BT_{4\text{-}FW\text{-}90\text{-}H}$, and $BT_{6\text{-}FW\text{-}90\text{-}H}$ obtained the highest gains in shear capacity of 167, 163, and 169%, respectively. Moreover, the mid-span deflection at ultimate load for the aforementioned beams was significantly increased due to the propagation of flexural cracks as the developed load increased. Consequently, the gains in ductility of specimens $BT_{6\text{-}UW\text{-}90\text{-}H}$, $BT_{4\text{-}FW\text{-}90\text{-}H}$, and $BT_{6\text{-}FW\text{-}90\text{-}H}$ were the best compared to control beam BC2 as well as other strengthened specimens, and equal to 234, 313, and 314%, respectively. Although side-bonded and U-wrapped strengthened RC beams achieved lower shear capacities and ductility indexes compared to fully-wrapped specimens, the gains in both ultimate load and ductility considerably improved when the number of GFTM layers within the strengthening strips increased. The gain in shear capacity of side-bonded strengthened RC beams was in the range of 32%-91%, while their U-wrapped counterparts were in the range of 101%-167% compared to BC2. Additionally, both side-bonded and U-wrapped strengthened beams failed with a sufficient ductility index, even though the recorded values were much lower than fully-wrapped specimens. The gains in ductility compared to BC2 of side-bonded, U-wrapped, and fully-wrapped strengthened RC beams were in the range of 86–99%, 95–234%, and 186–314%, respectively.

6. Summary and conclusion

This paper investigated experimentally and numerically the shear performance of RC beams strengthened using GFTM-SHCC strips. Thirteen half-scale simply supported RC beams were tested to explore the effects of the layers' number of the GFTM layers within the SHCC strips, the spacing between the strengthening strips, orientations and configurations of the strengthening system, and the location of the strengthening strips relative to the internal stirrups on the shear performance. Moreover, a 3D non-linear FEM was constructed using ABAQUS software and verified against the experimental records to numerically run a parametric study in order to compare between intermittent strengthening using GFTM-SHCC strips and the whole continuous strengthening of the critical shear span zone. Based on the discussions described in the current research, the following conclusions can be drawn:.

1. The proposed technique of casting the GFTM-SHCC strengthening strips inside grooves of 20 mm within the web of the RC beams efficiently prevented the debonding between the substrate RC beam and the strengthening strips.
2. The shear capacity and ductility of intermittently strengthened RC beams were significantly enhanced compared to the reference specimens. The gains in the shear capacity and the ductility of the intermittent GFTM-SHCC strips strengthened RC beams were in the range of 47–142% and 21–172%, respectively.
3. As the number of the GFTM layers inside SHCC strips increased, the cracking load was delayed and the ultimate shear capacity and ductility index improved.
4. The results of the tests of the RC beams strengthened with different spacing between the GFTM-SHCC strips declared that the spacing between the strips did not significantly affect the cracking load of the strengthened specimens. Quite the contrary, the gain in ultimate shear capacity was considerable (105%) when a small spacing (90 mm) between the strengthening strips was suggested. The concrete was effectively confined at the critical shear zone due to the small spacing between the SHCC strips.
5. Fully-wrapped strengthened RC beams exhibited higher gains in shear capacity and ductility with respect to side-bonded and U-wrapped specimens.
6. RC beams strengthened with U-wrapped inclined GFTM-SHCC strips with an orientation angle of 45° and 60° to the axis of the beam had a remarkable improvement in the cracking and ultimate loads compared to 90° (vertical strips).
7. RC specimens with web reinforcement in the critical shear span and strengthened with GFTM-SHCC strips recorded the highest shear load among all strengthened specimens. Moreover, GFTM-SHCC strips unaligned with the inner web reinforcements were more efficient than the strengthening strips at the same location of the stirrup legs.
8. The numerical results showed that strengthening of the whole critical shear span zone efficiently delayed the rupture of the strengthening strips and led to a significant increase in the ultimate carrying load capacity and mid-span deflection at failure with respect to intermittent strengthening.

Data availability

The raw data required to reproduce these findings are available only with direct contact through email to the corresponding author. The processed data required to reproduce these findings are available only with direct contact through email to the corresponding author.

Funding

The author(s) received no financial support for the research, authorship, and/or publication of this article.

Declaration of Competing Interest

The authors declare that they have no known competing financial interests or personal relationships that could have appeared to influence the work reported in this paper.

References

[1] Sakr, M.A., Sleemah, A.A., Khalifa, T.M. and Mansour, W.N., 2018. Behavior of RC beams strengthened in shear with ultra-high performance fiber reinforced concrete (UHPFRC). In MATEC web of conferences (Vol. 199, p. 09002). EDP Sciences. 10.1051/matecconf/201819909002.

[2] J.H. Gonzalez-Libreros, C. Sabau, L.H. Sneed, C. Pellegrino, G. Sas, State of research on shear strengthening of RC beams with FRCM composites, Constru. Build. Mater. 149 (2017) 444–458, https://doi.org/10.1016/j.conbuildmat.2017.05.128.

[3] Brückner, A., Ortlepp, R. and Curbach, M., 2006. Textile reinforced concrete for strengthening in bending and shear. Materials and structures, 39(8), pp.741-748. [3] Bruckner A, Ortlepp R, Curbach M. Textile reinforced concrete for strengthening in bending and shear. Mater. Struct 2006; 39: 741–748. 10.1617/14283.

[4] A. Brückner, R. Ortlepp, M. Curbach, Anchoring of shear strengthening for T-beams made of textile reinforced concrete (TRC), Materials and Structures 41 (2) (2008) 407–418, https://doi.org/10.1617/s11527-007-9254-9.

[5] R. Contamine, A.S. Larbi, P. Hamelin, Identifying the contributing mechanisms of textile reinforced concrete (TRC) in the case of shear repairing damaged and reinforced concrete beams, Engineering Structures 46 (2013) 447–458, https://doi.org/10.1016/j.engstruct.2012.07.024.

[6] Triantafillou, T.C., Papanicolaou, C.G., Zissimopoulos, P. and Laourdekis, T., 2006. Concrete confinement with textile-reinforced mortar jackets. ACI structural journal, 103(1), p.28. 10.14359/15083.

[7] C. Escrig, L. Gil, E. Bernat-Maso, F. Puigvert, Experimental and analytical study of reinforced concrete beams shear strengthened with different types of textile-reinforced mortar, Constr. Build. Mater. 83 (2015) 248–260, https://doi.org/10.1016/j.conbuildmat.2015.03.013.

[8] L.N. Koutas, Z. Tetta, D.A. Bournas, T.C. Triantafillou, Strengthening of concrete structures with textile reinforced mortars: state-of-the-art review, J. Compos. Constr. 23 (1) (2019) 03118001, https://doi.org/10.1061/(asce)cc.1943-5614.0000882.

[9] Tayeh, B.A., Aadi, A.S., Hilal, N.N., Bakar, B.A., Al-Tayeb, M.M. and Mansour, W. N., 2019, September. Properties of ultra-high-performance fiber-reinforced concrete (UHPFRC)-a review paper. In AIP Conference Proceedings (Vol. 2157, No. 1, p. 020040). AIP Publishing LLC.

[10] S. Fayed, W. Mansour, Evaluate the effect of steel, polypropylene and recycled plastic fibers on concrete properties, Adv. Concr. Constru. 10 (4) (2020) 319–332.

[11] W. Mansour, B.A. Tayeh, Shear behaviour of RC beams strengthened by various ultrahigh performance fibre-reinforced concrete systems, Adv. Civil Eng. 2020 (2020), https://doi.org/10.1155/2020/2139054.

[12] A. Basha, S. Fayed, W. Mansour, Flexural strengthening of RC one-way solid slab with Strain Hardening Cementitious Composites (SHCC), Adv. Concr. Constr. 9 (5) (2020) 511–527.

[13] W. Mansour, M. Sakr, A. Seleemah, B.A. Tayeh, T. Khalifa, Development of shear capacity equations for RC beams strengthened with UHPFRC, Computers and Concrete 27 (5) (2021) 473–487.

[14] T. Blanksvärd, B. Täljsten, A. Carolin, Shear strengthening of concrete structures with the use of mineral-based composites, J. Compos. Constr. 13 (1) (2009) 25–34, https://doi.org/10.1061/(asce)1090-0268(2009)13:1(25).

[15] Z.R. Aljazaeri, M.A. Janke, J.J. Myers, A novel and effective anchorage system for enhancing the flexural capacity of RC beams strengthened with FRCM composites, Composite Structures 210 (2019) 20–28, https://doi.org/10.1016/j.compstruct.2018.10.110.

[16] M.Y. Alabdulhady, L.H. Sneed, C. Carloni, Torsional behavior of RC beams strengthened with PBO-FRCM composite-An experimental study, Engineering Structures 136 (2017) 393–405, https://doi.org/10.1016/j.engstruct.2017.01.044.

[17] T.G. Wakjira, U. Ebead, Hybrid NSE/EB technique for shear strengthening of reinforced concrete beams using FRCM: Experimental study, Constr. Build. Mater. 164 (2018) 164–177, https://doi.org/10.1016/j.conbuildmat.2017.12.224.

[18] E. Tzoura, T.C. Triantafillou, Shear strengthening of reinforced concrete T-beams under cyclic loading with TRM or FRP jackets, Materials and Structures 49 (1) (2016) 17–28, https://doi.org/10.1617/s11527-014-0470-9.

[19] Z.C. Tetta, L.N. Koutas, D.A. Bournas, Textile-reinforced mortar (TRM) versus fiber-reinforced polymers (FRP) in shear strengthening of concrete beams, Composites Part B: Engineering 77 (2015) 338–348, https://doi.org/10.1016/j.compositesb.2015.03.055.

[20] S.M. Raoof, L.N. Koutas, D.A. Bournas, Textile-reinforced mortar (TRM) versus fibre-reinforced polymers (FRP) in flexural strengthening of RC beams, Constr. Build. Mater. 151 (2017) 279–291, https://doi.org/10.1016/j.conbuildmat.2017.05.023.

[21] T. Trapko, D. Urbańska, M. Kamiński, Shear strengthening of reinforced concrete beams with PBO-FRCM composites, Composites Part B: Engineering 80 (2015) 63–72, https://doi.org/10.1016/j.compositesb.2015.05.024.

[22] T. Triantafillou, C. Papanicolaou, Shear Strengthening of Reinforced Members with Textile Reinforced Mortar (TRM) Jackets, J. Compos. Constr. 2 (2005) 96–104, https://doi.org/10.1617/14308.

[23] Z.R. Aljazaeri, J.J. Myers, Strengthening of reinforced-concrete beams in shear with a fabric-reinforced cementitious matrix, J. Compos. Constr. 21 (5) (2017) 04017041, https://doi.org/10.1061/(asce)cc.1943-5614.0000822.

[24] R. Azam, K. Soudki, FRCM strengthening of shear-critical RC beams, J. Compos. Constr. 18 (5) (2014) 04014012, https://doi.org/10.1061/(asce)cc.1943-5614.0000464.

[25] A. Younis, U. Ebead, K.C. Shrestha, Different FRCM systems for shear-strengthening of reinforced concrete beams, Constr. Build. Mater. 153 (2017) 514–526, https://doi.org/10.1016/j.conbuildmat.2017.07.132.

[26] R. Azam, K. Soudki, J.S. West, M. Noël, Behavior of shear-critical RC beams strengthened with CFRCM, J. Compos. Constr. 22 (1) (2018) 04017046, https://doi.org/10.1061/(asce)cc.1943-5614.0000829.

[27] J.H. Gonzalez-Libreros, L.H. Sneed, T. D'Antino, C. Pellegrino, Behavior of RC beams strengthened in shear with FRP and FRCM composites, Engineering Structures 150 (2017) 830–842, https://doi.org/10.1016/j.engstruct.2017.07.084.

[28] Y.Z. Zheng, W.W. Wang, K.M. Mosalam, Q. Fang, L. Chen, Z.F. Zhu, Experimental investigation and numerical analysis of RC beams shear strengthened with FRP/ECC composite layer, Composite Structures 246 (2020), 112436, https://doi.org/10.1016/j.compstruct.2020.112436.

[29] Y.A. Al-Salloum, H.M. Elsanadedy, S.H. Alsayed, R.A. Iqbal, Experimental and numerical study for the shear strengthening of reinforced concrete beams using textile-reinforced mortar, J. Compos. Constr. 16 (1) (2012) 74–90, https://doi.org/10.1061/(asce)cc.1943-5614.0000239.

[30] F. Hosseini, B. Gencturk, S. Lahpour, D.I. Gil, An experimental investigation of innovative bridge columns with engineered cementitious composites and Cu–Al–Mn super-elastic alloys, Smart Materials and Structures 24 (8) (2015), 085029, https://doi.org/10.1088/0964-1726/24/8/085029.

[31] X. Wu, T.H.K. Kang, Y. Lin, H.J. Hwang, Shear strength of reinforced concrete beams with precast High-Performance Fiber-Reinforced Cementitious Composite permanent form, Composite Structures 200 (2018) 829–838, https://doi.org/10.1016/j.compstruct.2018.06.007.

[32] H.M. Afefy, A.T. Baraghith, M.H. Mahmoud, Retrofitting of defected reinforced-concrete cantilever slabs using different techniques, Magazine of Concrete Research 72 (14) (2020) 703–719, https://doi.org/10.1680/jmacr.18.00340.

[33] A.B. Elnagar, H.M. Afefy, A.T. Baraghith, M.H. Mahmoud, Experimental and numerical investigations on the impact resistance of SHCC-strengthened RC slabs subjected to drop weight loading, Constr. Build. Mater. 229 (2019), 116866, https://doi.org/10.1016/j.conbuildmat.2019.116866.

[34] M.H. Mahmoud, H.M. Afefy, A.T. Baraghith, A.B. Elnagar, Impact and static behavior of strain-hardening cementitious composites–strengthened reinforced concrete slabs, Adv. Struct. Eng. 23 (8) (2020) 1614–1628, https://doi.org/10.1177/1369433219898099.

[35] Z. Ding, J. Wen, X. Li, J. Fu, X. Ji, Mechanical behaviour of polyvinyl alcohol-engineered cementitious composites (PVA-ECC) tunnel linings subjected to vertical load, Tunnelling and Underground Space Technology 95 (2020), 103151, https://doi.org/10.1016/j.tust.2019.103151.

[36] A. Hassan, A.T. Baraghith, A.M. Atta, T.F. El-Shafiey, Retrofitting of shear-damaged RC T-beams using U-shaped SHCC jacket, Engineering Structures 245 (2021), 112892, https://doi.org/10.1016/j.engstruct.2021.112892.

[37] H.M. Afefy, A.T. Baraghith, A. Hassan, M.K. Abuzaid, Strengthening of shear-deficient RC beams using near surface embedded precast cement-based composite plates (PCBCPs), Engineering Structures 244 (2021), 112765, https://doi.org/10.1016/j.engstruct.2021.112765.

[38] Egyptian code for design and construction of reinforced concrete structures (ECP 203-2018), Housing and Building National Research Center, Cairo, Egypt. 2018.

[39] International Society for Rock Mechanics (ISRM). Commission on standardization of laboratory and field tests., suggested methods for determining tensile strength of rock materials. Int J Rock Mech Min Sci 1978;15:99–103.

[40] ASTM C1609 / C1609M-19a, Standard test method for flexural performance of fiber-reinforced concrete (using beam with third-point loading), ASTM International, Pennsylvania, USA, 2010. DOI: 10.1520/C1609_C1609M-19A.

[41] M.A. Sakr, A.A. Sleemah, T.M. Khalifa, W.N. Mansour, Shear strengthening of reinforced concrete beams using prefabricated ultra-high performance fiber reinforced concrete plates: Experimental and numerical investigation, Structural Concrete 20 (3) (2019) 1137–1153, https://doi.org/10.1002/suco.201800137.

[42] ASTM-C496. Splitting tensile strength of cylindrical concrete. West Conshohocken, PA 19428-2959. 1996. 10.1520/c0496-96.

[43] Sprinkel, M.M. and Ozyildirim, C., 2000. Evaluation of high performance concrete overlays placed on Route 60 over Lynnhaven Inlet in Virginia (No. VTRC-01-R1). Virginia Transportation Research Council. 10.3141/1610-03.
[44] Mansour, W. and Fayed, S., 2021, February. Effect of interfacial surface preparation technique on bond characteristics of both NSC-UHPFRC and NSC-NSC composites. In Structures (Vol. 29, pp. 147-166). Elsevier. 10.1016/j.istruc.2020.11.010.
[45] ASCE-ACI Committee 445 on Shear and Torsion, 1998. Recent approaches to shear design of structural concrete. Journal of structural engineering, 124(12), pp.1375-1417. 10.1061/(asce)0733-9445(1998)124:12(1375).
[46] B. Li, E.S.S. Lam, B. Wu, Y.Y. Wang, Experimental investigation on reinforced concrete interior beam–column joints rehabilitated by ferrocement jackets, Engineering Structures 56 (2013) 897–909, https://doi.org/10.1016/j.engstruct.2013.05.038.
[47] A.E.H. Khalil, E. Etman, A. Atta, A. Baraghith, R. Behiry, The effective width in shear design of wide-shallow beams: a comparative study, KSCE J. Civil Eng. 23 (4) (2019) 1670–1681, https://doi.org/10.1007/s12205-019-0830-7.
[48] ACI Committee, 2019. Building code requirements for structural concrete (ACI 318-19) and commentary. American Concrete Institute, Farmington Hills, MI, 519 ppfv. 10.14359/51716937.
[49] Japan Society of Civil Engineers. Recommendations for design and construction of high-performance fiber reinforced cement composite with multiple fine cracks (HPFRCC). Concrete engineering series 82, 2008.
[50] K. Hibbitt, Sorensen: ABAQUS Theory manual, Version 6.1, Hibbitt, Karlsson and Sorensen, Pawtucket, 2000.
[51] V. Birtel, P. Mark, Parameterised Finite Element Modelling of RC Beam Shear Failure, In ABAQUS users' conference (2007) 95–108.
[52] Sanez lp. Discussion of equation for the stress - strain curve of concrete by desayi and krishnan. ACI journal.1964; 61:1229-1235. 10.14359/7785.
[53] H.-T. Hu, W.C. Schnobrich, Constitutive modelling of concrete by using nonassociated plasticity, J. Mater. Civil Eng. (ASCE) 1 (4) (1989) 199–216, https://doi.org/10.1061/(ASCE)0899-1561(1989)1:4(199).
[54] A. Ganganagoudar, T.G. Mondal, S.S. Prakash, Improved softened membrane model for reinforced concrete circular bridge columns under torsional loading, J. Bridge Eng. 21 (7) (2016) 04016037, https://doi.org/10.1061/(asce)be.1943-5592.0000907.
[55] W. Mansour, Numerical analysis of the shear behavior of FRP-strengthened continuous RC beams having web openings, Engineering Structures 227 (2021), 111451, https://doi.org/10.1016/j.engstruct.2020.111451.